AD-A046 315 BROWN UNIV PROVIDENCE R I DIV OF ENGINEERING F/G 9/1
A STUDY OF FERRITE LOADED PLANAR WAVEGUIDING STRUCTURES,(U)
MAR 77 D M BOLLE N00014-75-C-0750
UNCLASSIFIED NL

| OF |
AD
A046 315

END
DATE
FILMED
12-77
DDC

Division of Engineering
BROWN UNIVERSITY
PROVIDENCE, R. I.

A STUDY OF FERRITE LOADED PLANAR WAVEGUIDING STRUCTURES

Donald M. Bolle

Department of the Navy
Office of Naval Research
Contract N00014-75-C-0750
Technical Report No. 1

National Science Foundation
Washington, D. C.
Research Grant ENG74-14187

N00014-75-C-0750/1
ENG74-14187/1

March 1977

(6) A Study of Ferrite Loaded Planar Waveguiding Structures,

by

(10) Donald M. Bolle

Division of Engineering
Brown University
Providence, Rhode Island 02912

(11) March 1977

(12) 67 p.

Prepared for

The Office of Naval Research
and
The National Science Foundation

(15) This research was supported under ONR Contract N00014-75-C-0750 and NSF Grant-ENG 74-14187.

NSF-ENG 74-14187

INDEX

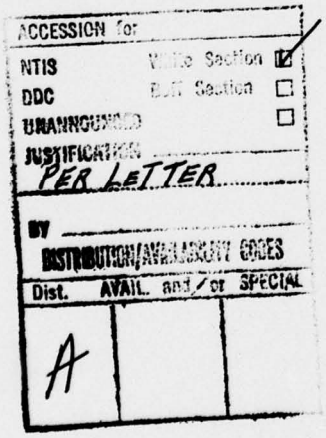

I. Summary

This report describes in detail the work performed on ferrite loaded planar waveguiding structures over the past two years, under sponsorship, in part, by the National Science Foundation through grant ENG 74-14187 and by the Office of Naval Research under contract N00014-75-C-0750.

The primary motivation for this research rested on the desire and need to understand clearly electromagnetic field displacement effects in inhomogeneously ferrite loaded planar waveguiding structures. An example of such a structure would be the microstrip line on a ferrite substrate or a ferrite loaded stripline.

M. E. Hines[2,4,5,14] pioneered a stripline isolator which used an 'edge-guided' mode and exhibited unusual broadband behavior. Much effort was also expended by workers in Italy, Japan, and France [6-13,15-22] to improve such devices particularly with regard to their insertion loss over the total operating band. Indifferent success met these efforts.

It became clear that a much stronger theoretical basis was needed before further progress could be made. This need provided the primary impetus for our work.

We examine and describe here the various canonical geometries for which exact solutions were obtained and which, recently, have led us to reject the 'edge-guided' mode, also known as the peripheral mode, as the primary agent in the device operation since the bandwidth of this magnetostatic mode does not, under any circumstances approach the bandwidth observed for devices using the field displacement effect. Instead, it now has become clear (refs. 23-25) that the normal quasi-TEM 'waveguide' mode is modified in the region where the effective permeability is negative (and even beyond this region) so as to take on a quasi-surface or edge-guided mode structure. Interestingly enough, however, the energy

concentration occurs at the interface opposite to the one supporting the edge-guided magnetostatic mode. It appears therefore that devices may concurrently support both modes which would lead to an increased insertion loss over that which would be expected if only one mode were excited.

In the following chapters we describe in essentially chronological order our work which has led to these conclusions. We start with the simplest model and develop our work so as to approach the final geometry of interest, the shielded microstrip line.

II: The Peripheral or Edge-Guided Mode

II (a) Introduction

The early debate concerning the use of the edge-guided mode in isolator phase shifter, and circulator component geometries centered on the nature of the mode. The precise nature of the mode and its relationship to other modes which may exist on the planar geometries employed in these devices was not clearly understood. For substantial advances to be made in the electrical performance of these devices it was felt necessary that a more complete and exact analysis be initiated. Such an analysis was felt to be particularly important because the initial broad band performance was sufficiently promising that considerable excitement was generated concerning the potential utility and application of these devices. However, the performance of the components that was achieved though yielding useful results, has not matched the very fine performance of the much narrower band isolators and circulators, for example.

The challenge was, and is, therefore to reach a sufficient understanding of the edge-guided modal system so that device performance can be substantially improved or, if not, that the inherent limitations are thoroughly understood.

To this end a study of several canonical geometries was initiated. The first, to be described here, is a geometry which, consisting of a single interface, can only support a surface type mode.

The direction of propagation is parallel to the dielectric-ferrite interface and the z-axis. (Fig. 1(a) and (b)).

To establish the nature of the surface modes which may exist on ferrite-dielectric interfaces with the d.c. magnetic biasing field tangential to the interfaces we consider the geometry of Fig. 1(a). To establish the relationship, if any, to the peripheral or edge-guided mode which exists on such

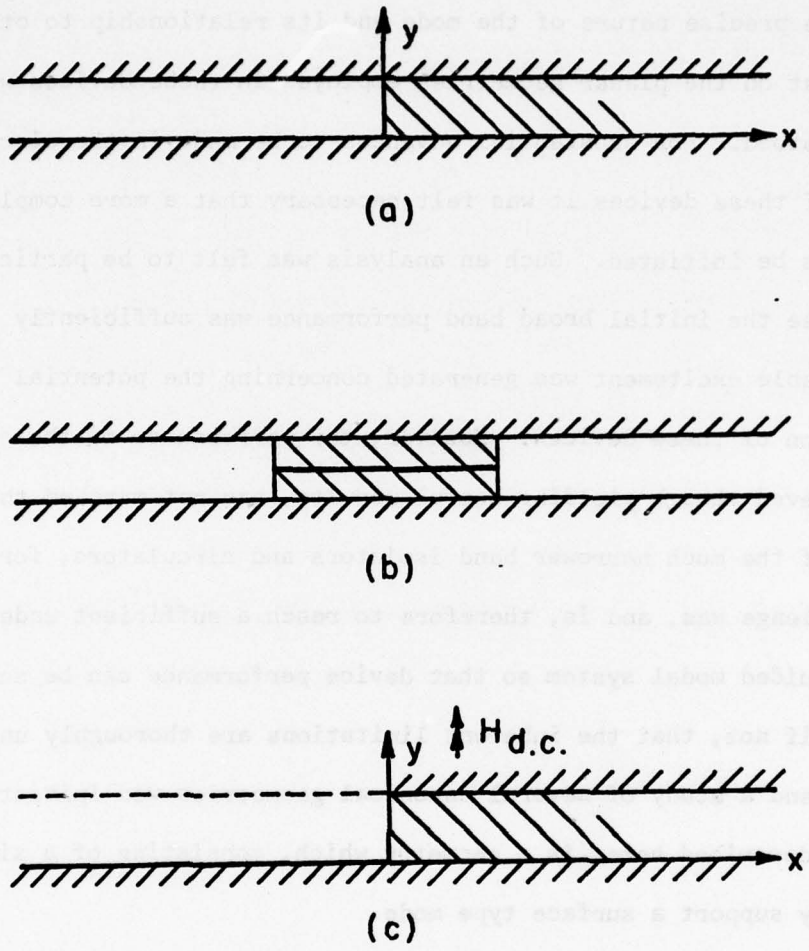

Figure 1 - Stripline geometries a) surface mode structure, b) ferrite loaded stripline geometry, c) canonical stripline geometry.

geometries as the ferrite loaded symmetric stripline of Fig. 1(b) we next consider the canonical geometry of Fig. 1(c) where the electric wall for $y = d$ $x < 0$ is replaced by a magnetic wall ($\underline{n} \times \underline{h} = 0$). It is assumed that the stripline is sufficiently wide so that the effect of the far edge is totally negligible.

II (b) Theory:

Contrary to the situation which pertains in isotropic media, where the transverse field components are most readily expressed in terms of the components of the field in the direction of propagation, in anisotropic media the components in the direction of the anisotropy axis turn out to be the most convenient for expressing the other field components.

From the Maxwellian equations the following general results are obtained for ferrite media

$$\Delta \underline{e}_t = -\delta'\gamma_1^2\Delta_t' e_y + j\kappa'\delta' \underline{a}_y \times \nabla_t' e_y$$

$$- j\kappa' \delta'^2 \nabla_t' h_y - \gamma_2^2 \underline{a}_y \times \nabla_t' h_y$$

$$\Delta \underline{h}_t = -j\kappa'\nabla_t' e_y - \gamma_1^2 \underline{a}_y \times \nabla_t' e_y + \delta'\gamma_1^2 \nabla_t' h_y - j\kappa'\delta' \underline{a}_y \times \nabla_t' h_y$$

and

$$(\nabla_t^2 + \gamma_2^2)\, e_y = +j\kappa'\delta' h_y$$

$$(\nabla_t^2 + \gamma_1^2)\, h_y = -j\kappa'\delta' e_y$$

i.e., the y-components of the field are coupled, and the permeability matrix for the ferrite medium is taken to be (29)

$$\mu = \mu_o \begin{bmatrix} 1+\chi & 0 & +j\kappa \\ 0 & 1+\chi & 0 \\ -j\kappa & 0 & 1 \end{bmatrix}$$

and

$$\chi = \frac{\omega_o \omega_m}{\omega_o^2 - \omega^2}$$

$$\kappa = -\frac{\omega \omega_m}{\omega_o^2 - \omega^2}$$

with

$$\omega_o = \gamma H_{d.c.} \qquad \omega_m = \gamma 4\pi M_s,$$

$H_{d.c.}$ being the d.c. magnetizing field magnitude and $4\pi M_s$ the saturation magnetization of the medium. The factor $e^{j(\omega t - \beta z)}$ will be suppressed throughout.

The above forms are obtained when we consider the case where the field components have the following dependency on the coordinate y.

$e_y, h_x, h_z \sim \cos \delta y$; $h_y, e_x, e_z \sim \sin \delta y$

We also have

$$\kappa' = \kappa/(1+\chi) \quad , \quad \beta' = \beta/k_f$$

$$\delta' = \delta/k_f, \quad k_f^2 = \omega^2 \mu_o \varepsilon_o \varepsilon_f$$

$$\gamma_1^2 = 1 - \delta'^2/(1+\chi)$$

$$\gamma_2^2 = 1+\chi - \frac{\kappa^2}{1+\chi} - \gamma'^2$$

$$\Delta = \gamma_1^4 - \frac{\kappa^2}{(1+\chi)}$$

$$\nabla_t' = \frac{1}{k} \nabla_t = \left(\underline{i}_x \frac{\partial}{\partial x'} + \underline{i}_z \frac{\partial}{\partial z'} \right)$$

and $x', y', z' = kx, ky, kz$

$$\underline{e} = j\underline{E} \qquad \underline{h} = \eta_f \underline{H} = \frac{\mu_o}{\varepsilon_f} H$$

Following Van Trier (28) the coupled wave equations may be uncoupled and the components e_y, h_y expressed in terms of the pair of scalar potentials which satisfy

$$(\nabla'^2 + \alpha_i^2)\, u_i = 0 \qquad i=1,2$$

where

$$\sigma_i^2 = + \frac{1}{2}(\gamma_1^2 + \gamma_2^2) \pm \sqrt{[\frac{1}{2}(\gamma_1^2 - \gamma_2^2)]^2 + (\kappa'\delta')^2}$$

For the y components of the field we obtain solutions of the form

$$e_y \sim e^{\alpha_i x'} \cos \delta y$$

$$jh_y \sim \zeta_i\, e^{\alpha_i x'} \sin \delta y$$

where

$$\alpha_i^2 = \beta^2 - \sigma_i^2$$

$$\zeta_i = \kappa'\delta' / (\gamma_1^2 - \alpha_1^2)$$

By replacing ε_f by $\acute{\varepsilon}_d$, say, and setting $\kappa = \chi = 0$ the expressions for an isotropic dielectric medium are recovered.

For an isotropic region the y-components decouple and take the form

$$e_y = \sum_n E_n\, e^{-\alpha_{0,n} x''} \cos \delta'' y \qquad x'' < 0$$

$$jh_y = \sum_n H_n\, e^{-\alpha_{0,n} x''} \sin \delta'' y$$

The other field components in the ferrite region may now be written in the form ($x \geq 0$).

$$e_x = \sum_n (a_n \theta_{1,n} e^{\alpha_{1,n} x'} + b_n \theta_{2,n} e^{\alpha_{2,n} x'}) \sin \delta y$$

$$jh_x = \sum_n (a_n \phi_{1,n} e^{\alpha_{1,n} x'} + b_n \phi_{2,n} e^{\alpha_{2,n} x'}) \cos \delta y$$

$$je_z = \sum_n (a_n \tau_{1,n} e^{\alpha_{1,n} x'} + b_n \tau_{2,n} e^{\alpha_{2,n} x'}) \sin \delta y$$

$$h_z = \sum_n (a_n \rho_{1,n} e^{\alpha_{1,n} x'} + b_n \rho_{2,n} e^{\alpha_{2,n} x'}) \cos \delta y$$

$$\theta_{i,n} = -\delta'_n \gamma^2_{1,n} \alpha_{i,n} - \beta' \gamma^2_{2,n} \zeta_{i,n} + \kappa'(\delta'^2_n \zeta_{i,n} \alpha_{i,n} + \delta'_n \beta')$$

$$\phi_{i,n} = \kappa'(\alpha_{i,n} + \beta' \delta'_n \zeta_{i,n}) - \gamma^2_{1,n}(\beta' + \delta'_n \zeta_{i,n} \alpha_{i,n})$$

$$\tau_{i,n} = \kappa' \delta'_n (\alpha_{i,n} + \beta' \delta'_n \zeta_{i,n}) - \beta' \delta'_n \gamma^2_{2,n} \zeta_{i,n} \alpha_{i,n}$$

$$\rho_{i,n} = -\kappa'(\beta' + \delta'_n \zeta_{i,n} \alpha_{i,n}) + \gamma^2_{1,n}(\alpha_{i,n} + \beta' \delta_n \zeta_{i,n})$$

Solutions are sought in which the $\alpha^2_{i,n}$ are positive. If $\alpha^2_{i,n}$ were to become negative or complex this would indicate that the fields no longer adhere either to an interface or to an edge at $x' = 0$.

The above expressions may be adapted to the particular regions which occur in the geometries of figure 1. In every case a solution is obtained by insisting on the continuity of the field components which lie in the plane $x' = 0$ for $0<y<d$.

The above expressions simplify considerable for the simple case of Fig. 1(a) where the single eigenfunctions suffice to yield the surface mode.

For the lowest order mode, we have no y-dependence whereas the higher order modes have a y dependency $\begin{Bmatrix}\sin\\ \cos\end{Bmatrix} \delta y$, $\delta = n\pi/d$. We further restrict ourselves to modes which adhere to the interface and therefore have a transverse behavior of the form $e^{-\alpha_{i,n}|x|}$, with $\alpha_{i,n} > 0$.

Applying the appropriate boundary condition yields a transcendental expression which relates the propagation constant β to the various electric and geometric parameters.

For the surface modes we obtain

$$\begin{vmatrix} +1 & 0 & -1 & -1 \\ 0 & \sqrt{\varepsilon_d/\varepsilon_f} & -\zeta_{1,n} & -\zeta_{2,n} \\ \tau_n^{(1)} & \rho_n^{(1)} & \tau_n^{(2)} & \rho_n^{(2)} \\ \rho_n^{(1)}\sqrt{\varepsilon_d/\varepsilon_f} & \tau_n^{(1)}\sqrt{\varepsilon_d/\varepsilon_f} & \nu_n^{(2)} & \mu_n^{(2)} \end{vmatrix} = 0, \quad n=0,1,2\ldots$$

where the superscript (1) and (2) refer to the dielectric and ferrite regions, respectively. The resulting expression simplifies considerably for the lowest order (n=0) mode.

We then obtain:

$$\frac{\alpha_f + \kappa'\beta'}{\mu_f} = -\alpha_d\sqrt{\varepsilon_d/\varepsilon_f}$$

where

$$\mu_f = (1+\chi) - \kappa^2/(1+\chi)$$
$$\alpha_d^2 = \beta^2 - \omega^2\mu_o\varepsilon_d$$
$$\alpha_f^2 = \beta^2 - \omega^2\mu_o\varepsilon_f\mu_f$$

Some further algebra generates the field components.

The theoretical treatment for the edge structure of Fig. 1(c) follows essentially the same pattern as that for the surface mode. However, in this case the modal structure must be modelled using an infinite series of eigenfunctions. The resulting algebra is considerably more cumbersome and leads to a dispersion relation which is an infinite determinant where the individual terms are themselves series. We must therefore determine at what point to terminate the series and when to truncate the determinant concurrently so as to avoid the usual numerical problems associated with this approach.

The expressions for the dispersion relation and the field components are cumbersome and will not be given in detail except to say that they follow the previous format.

II (c) Results:

Computer programs were written to yield, for both the surface mode and the edge-guided mode, the dispersion curves as well as the field components and the modal 'impedance' for the lowest order mode (n=0) only. The modal impedances were calculated three different ways, i.e., on voltage-current, power-current squared and voltage squared - power bases.

Figure 2 displays the three effective permeabilities which occur spontaneously within the theoretical treatment. The dominant one is shown by a solid line. The most significant region occurs for that range of frequencies for which the effective permeability becomes negative, for it is only in this range that surface modes occur in the geometry of Fig. 1(a).

Figure 3 shows the dispersion curve for the lowest order surface mode as a function of the permittivity of the dielectric region while Figure 4 shows the effect of changing the d.c. magnetic biasing field. These calculations for a lossless system shows clearly that the lower band of the mode lies at $f = \sqrt{f_o(f_o + f_m)}$ and that the system becomes highly dispersive well before we reach the limit of $f = f_o + f_m$. Figure 5 shows some results for the higher order modes, i.e., n=1 and 2, and illustrate their quite dispersive nature. Figure 6 and 7 give the dispersion curve and the impedance curves for a particular ferrite material and with the dielectric region having the same permittivity as the ferrite. The rapidly varying impedance over the surface mode bandwidth is clearly illustrated.

Figures 8 and 9 give the impedance as a function of frequency for the cases for which the dispersion curves are shown in Figures 3 and 4.

In Figure 10, we show the structure of the lowest order surface mode. Note that since the effective μ of the ferrite is negative the continuity of the

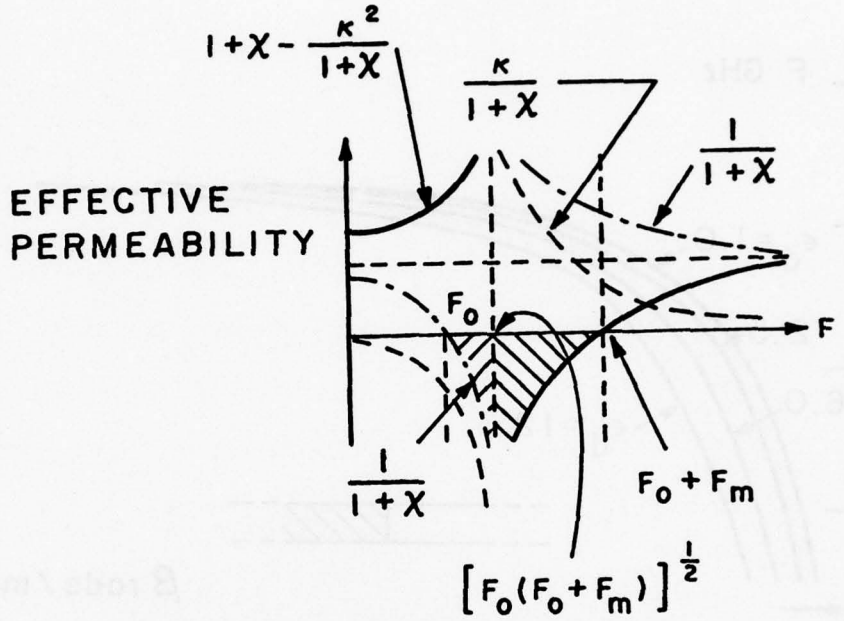

Figure 2 - Effective permeabilities as a function of frequency.

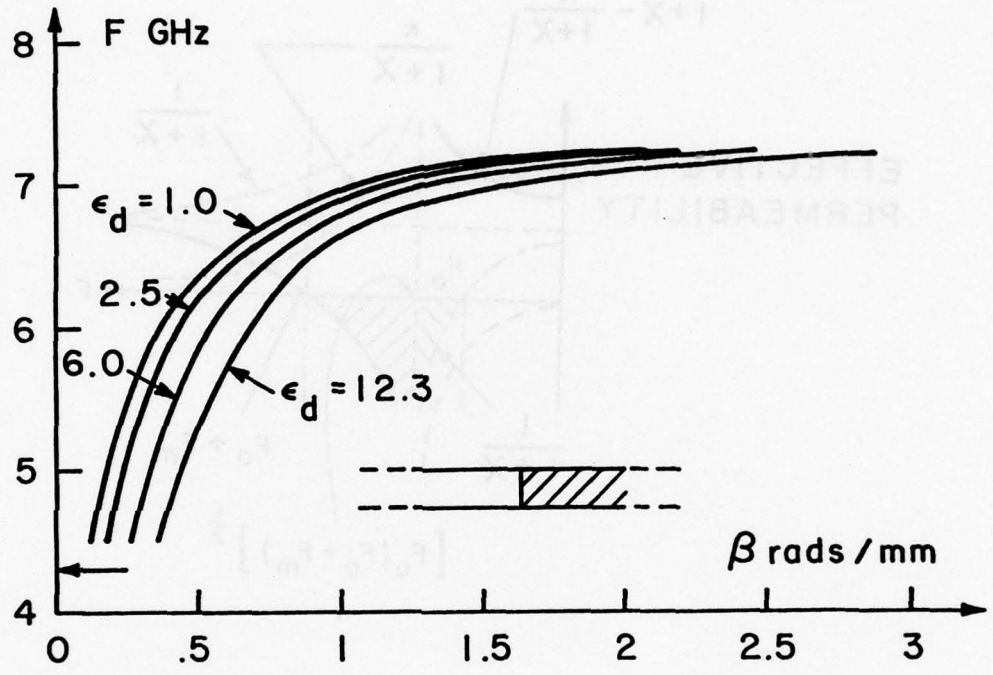

Figure 3 - Dispersion characteristics for the lowest order surface mode as a function of the permittivity of the dielectric region. Parameters are: $4\pi M_s$ = 4250 G., $H_{d.c.}$ = 1400 Oer., ϵ_f = 12.3, N=0.

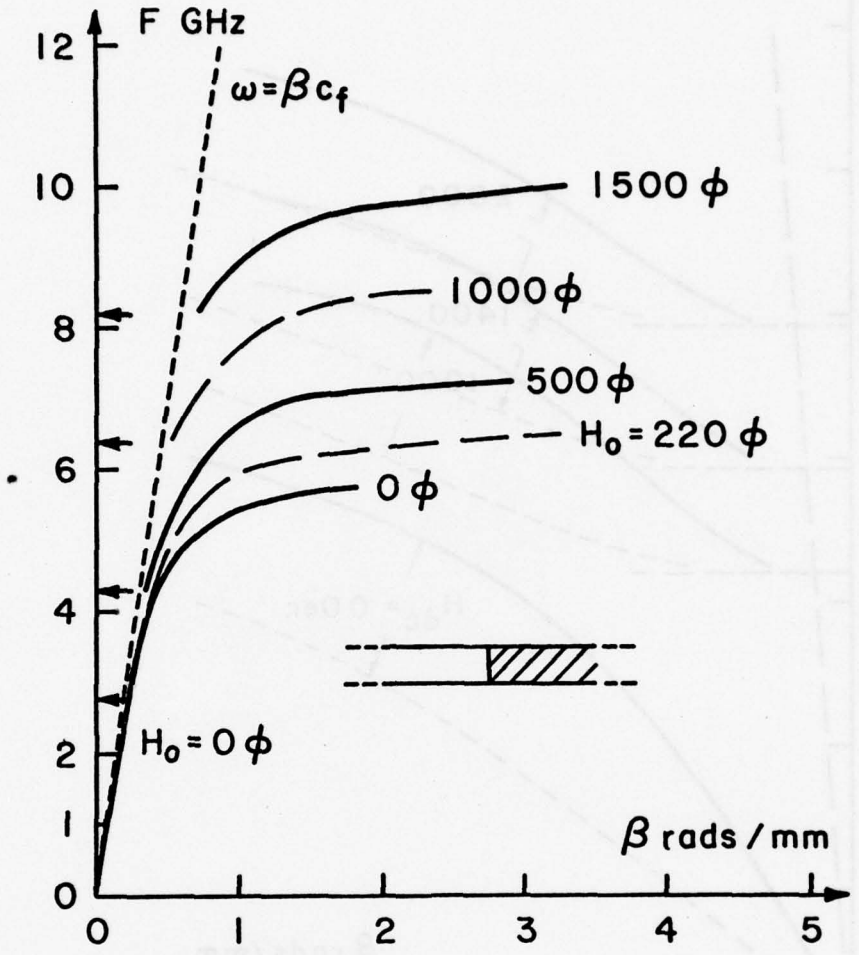

Figure 4 - Dispersion characteristics for the lowest order surface mode as a function of the d.c. biasing field. Parameters are $4\pi M_s$ = 4250 G., $\varepsilon_f = \varepsilon_d = 12.3$, N=0.

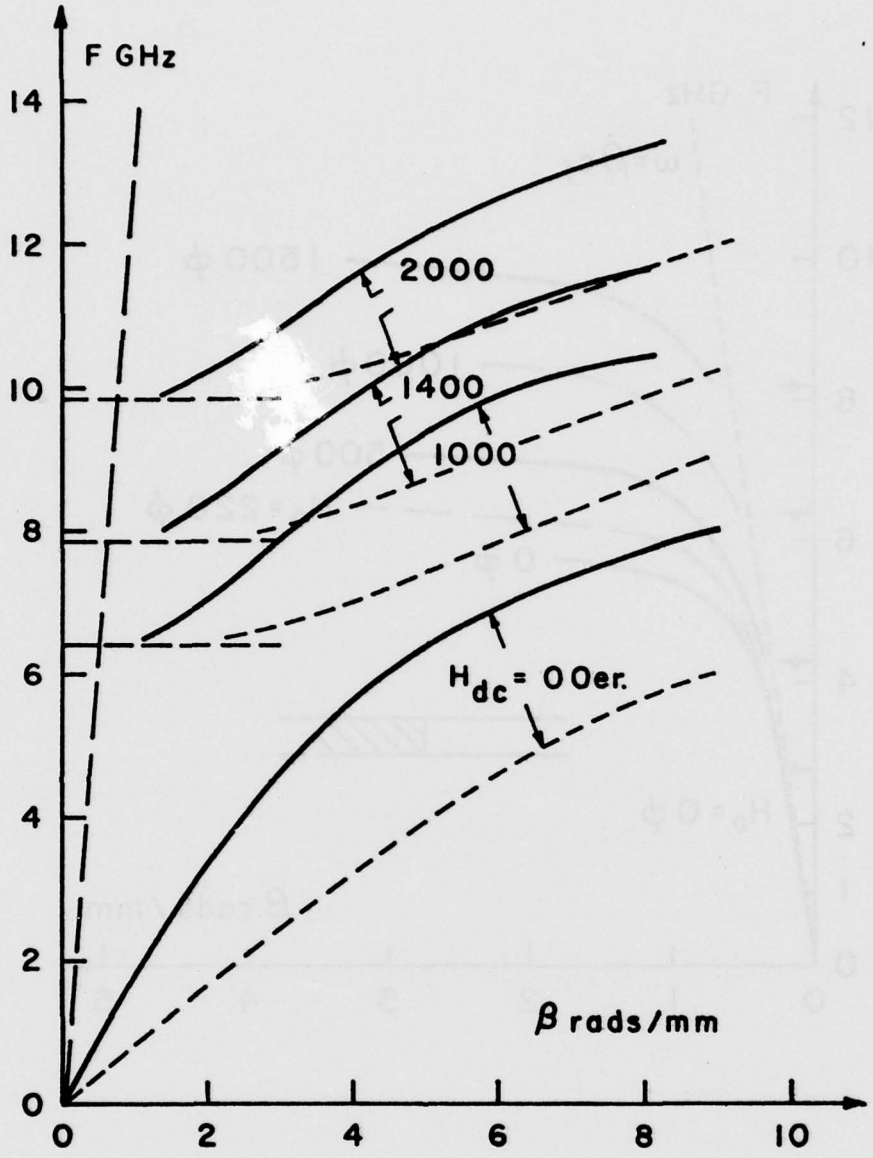

Figure 5 - Dispersion characteristics for the higher order surface modes as a function of the d.c. biasing field, (n=1 and 2). The parameters are: $4\pi M_s$ = 4250 G., ε_f = 12.3, ε_d = 1., d = 6 mm.
——— n=1, - - - - - -n=2, material resonance frequencies
$(F=\sqrt{F_o(F_o+F_m)})$

$4\pi M_s = 1780\,G \quad \epsilon_f = \epsilon_d = 14.5$

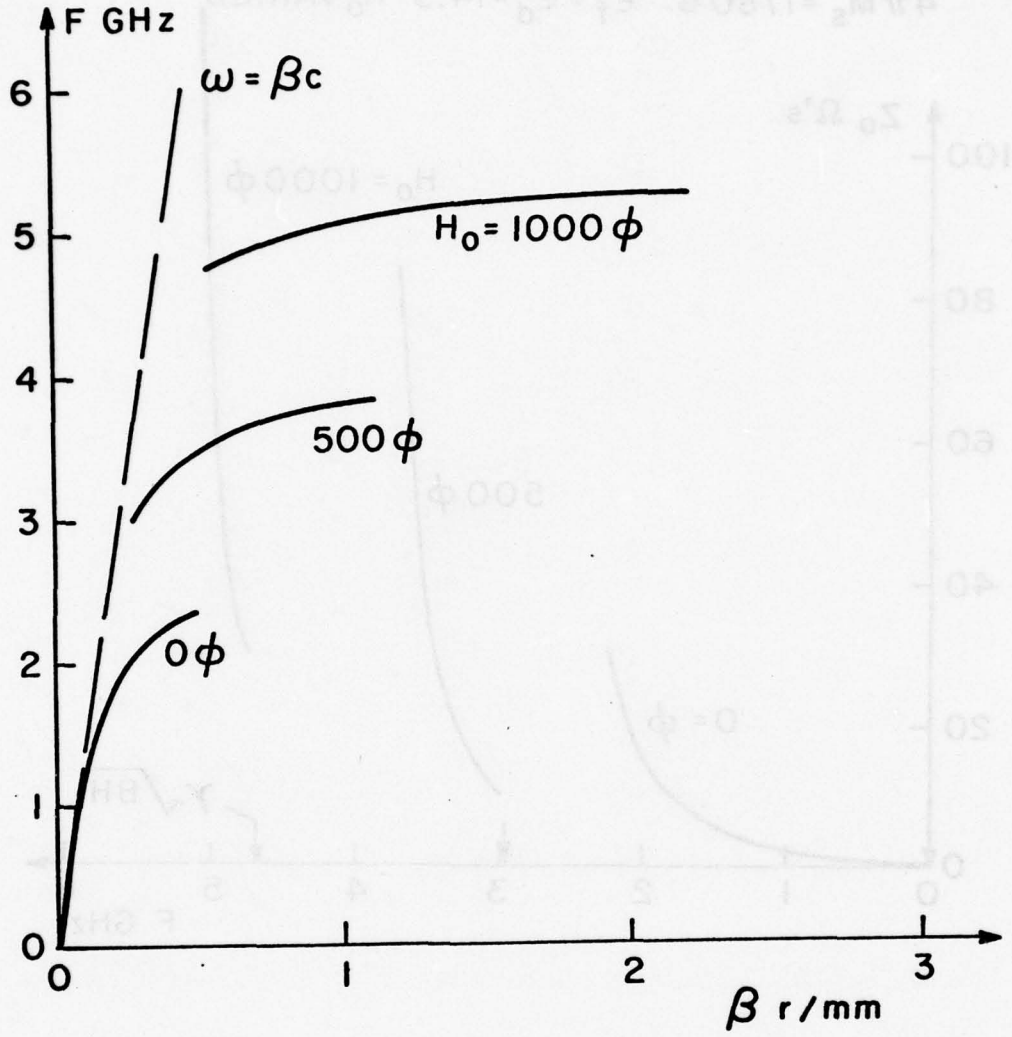

Figure 6 - Dispersion curves for the surface modes as a function of frequency. $4\pi M_s$ = 1780 Gauss, $\epsilon_f = \epsilon_d = 14.5$.

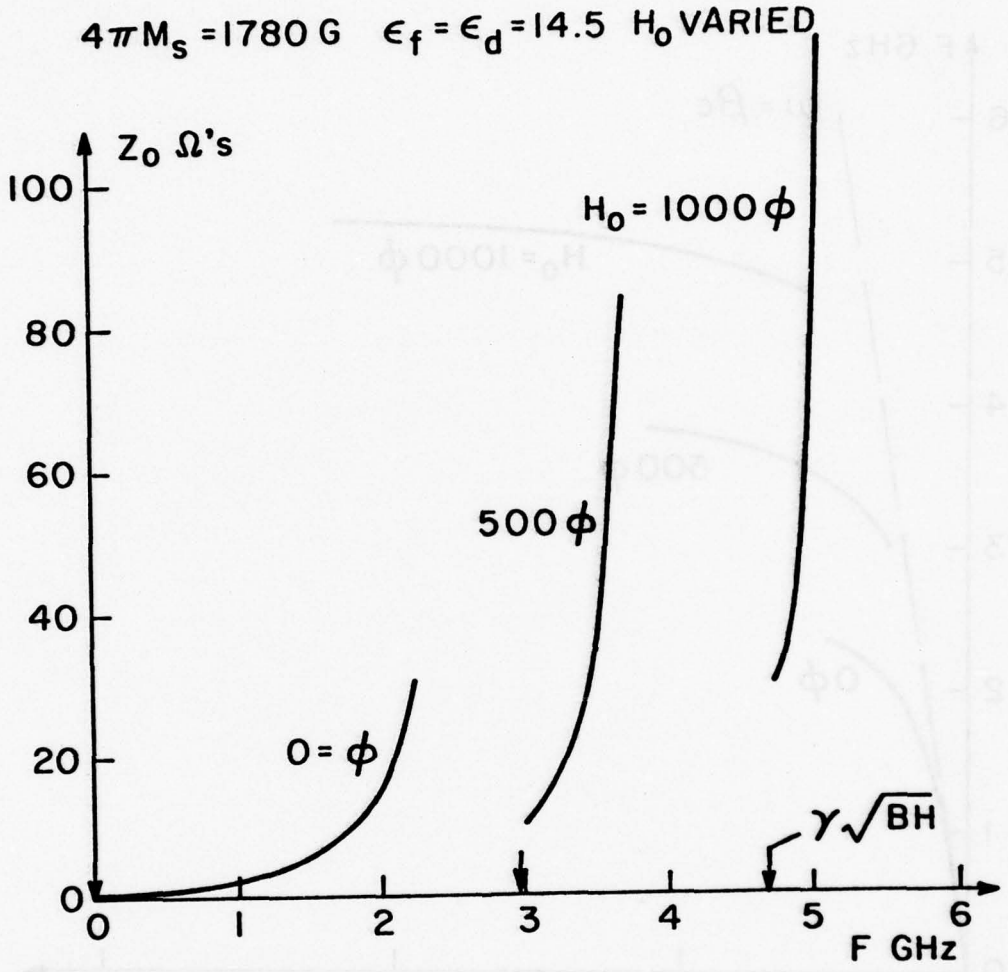

Figure 7 - The characteristic impedance of the surface mode as a function of frequency. Parameters as for Figure 6.

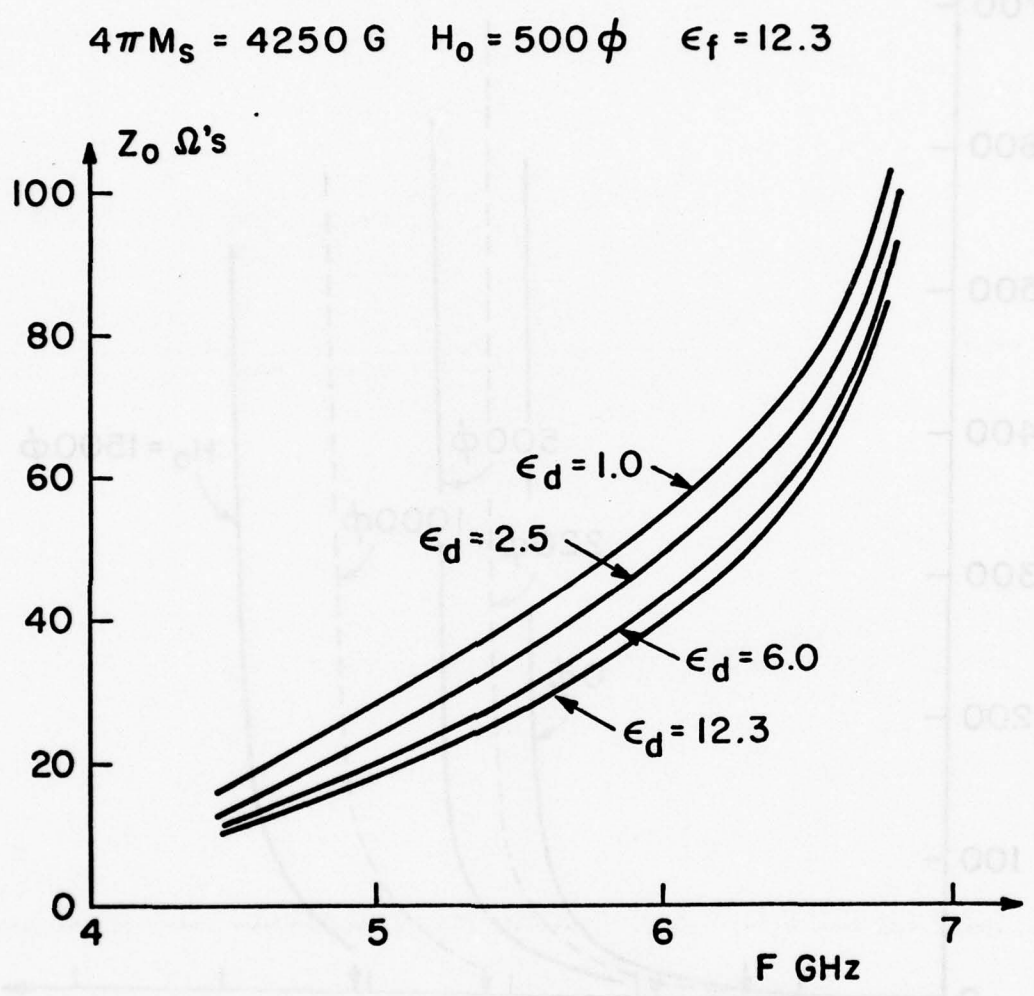

Figure 8 - **The characteristic impedance of the surface mode as a function of frequency and permittivity. Parameters as for Figure 3.**

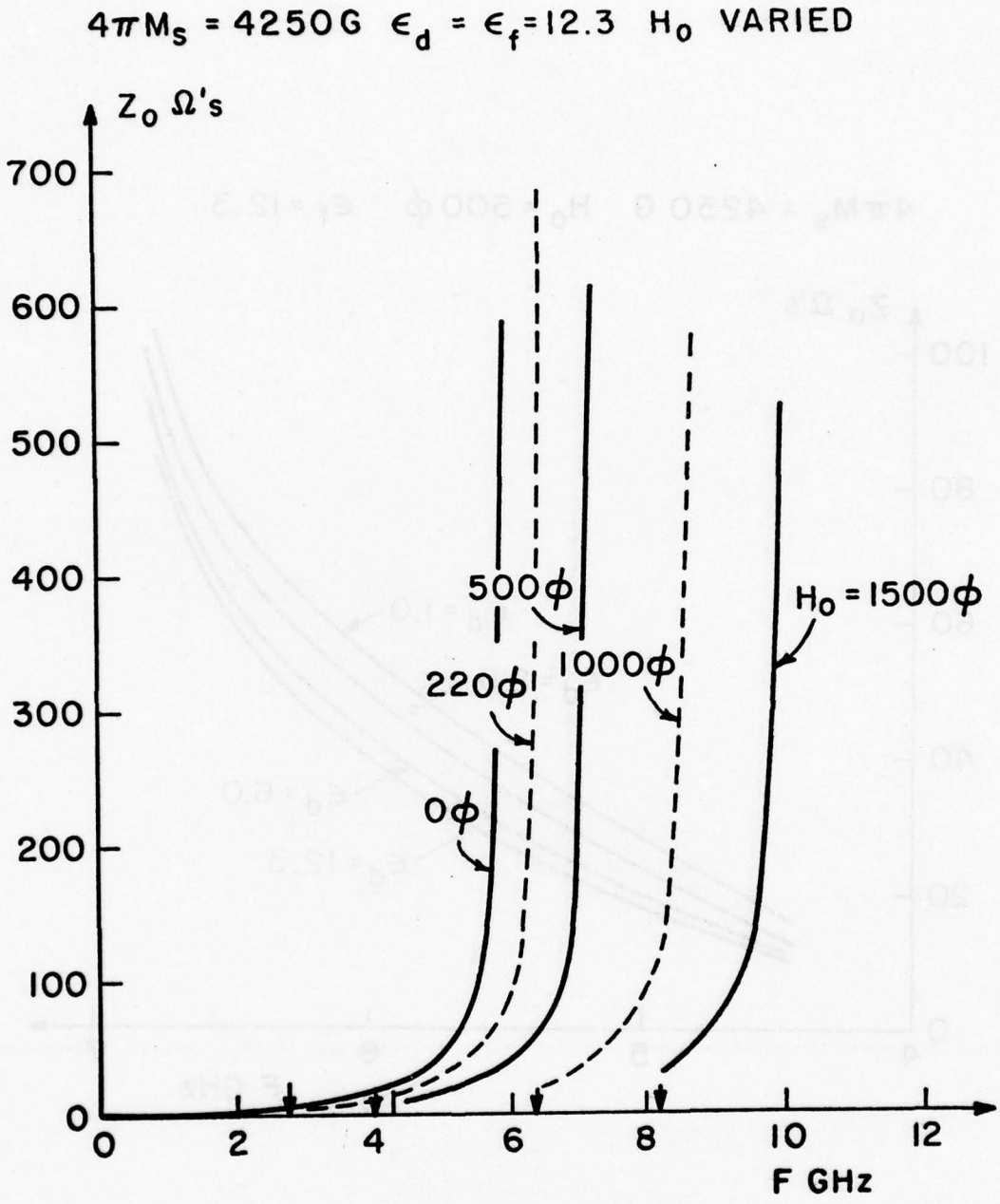

Figure 9 - The characteristic impedance of the surface mode as a function of frequency and d.c. magnetizing field. Parameters as for Fig. 4.

normal B component of the flux density (B_n) requires that the corresponding components of the magnetic field intensity are oppositely directed at the interface!

We now pass to the edge-guided modes and will present some results pertaining to the geometry of Figure 1(c). It was necessary first to determine the required size of the truncated determinant as well as the order to which the coefficient series had to be summed to achieve convergence and meet a required accuracy. Tests were run where the size of the truncated determinant was varied from 8 x 8 to 32 x 32 while the determinental coefficients were individually summed to up to 60 terms. For the worst case encountered an error of 5% resulted from using eight expansion coefficients in each series representation for the field and where the determinant entries were summed to twenty terms. Going to a (12/30) system reduced the error to about one percent while a (12/50) system resulted in an error of less than .1%. For generating much of the data for the following figures, a 5% accuracy was found to be adequate and was used out of economic considerations. For detailed studies, when necessary, a (12/50) search was employed. It should be indicated that using twelve terms in the field expansions leads to a (24 x 24) determinant since the fields in the ferrite require a two series representation, i.e., for $\alpha_{1,n}$ and $\alpha_{2,n}$!

In Figure 11 we show the lowest order edge-guided mode as a function of the permittivity of the dielectric region. We note that the effect of increasing the permittivity is to decrease the bandwidth of this mode. Figure 12 demonstrates the effect of changes in the d.c. magnetic biasing field. We note that reasonably broad band operation is available when materials with high saturation magnetization are employed and where the effective internal d.c. biasing field can be kept to low values. The bandwidth is therefore limited by the onset of

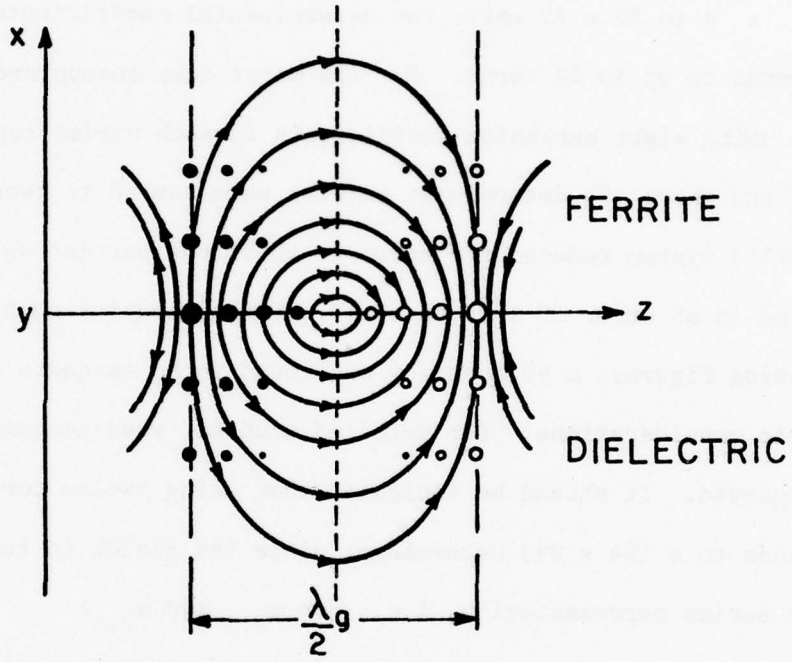

Figure 10 - Structure of the lowest order surface mode.

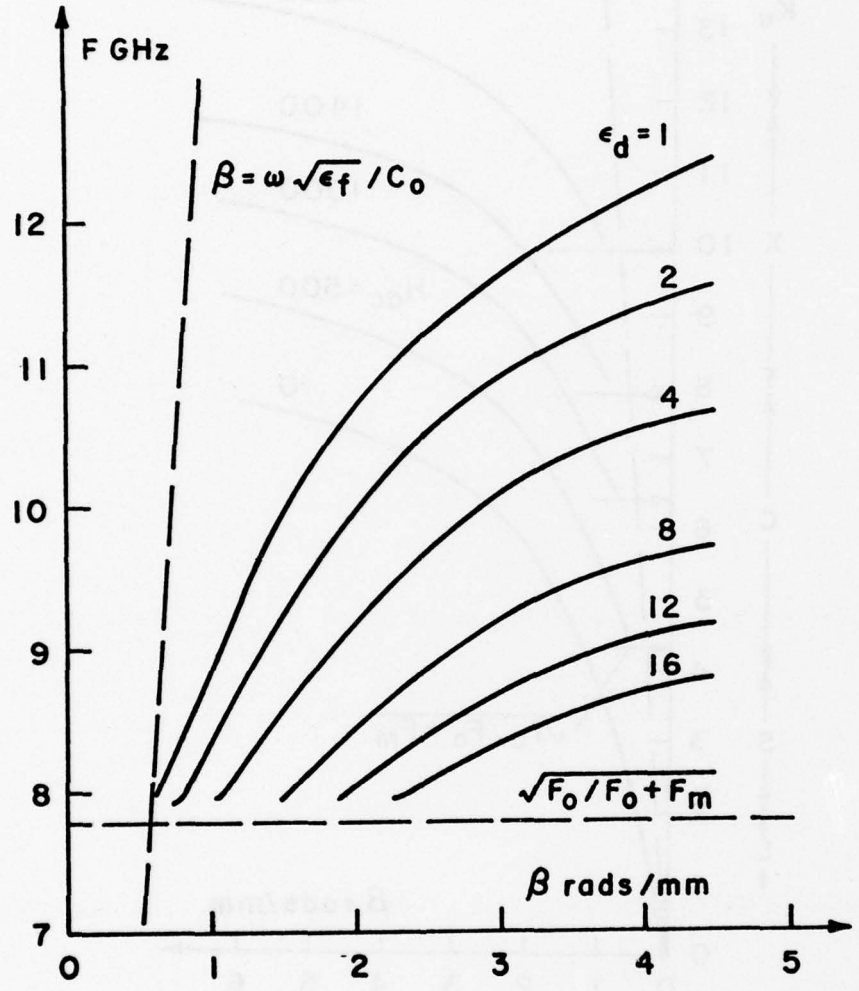

Figure 11 - The dispersion characteristics for the edge-guided mode for the geometry of Figure 1(c) as a function of the permittivity of the dielectrically loaded region. The parameters are: $4\pi M_s$ = 4250 G., $H_{d.c.}$ = 1400 Oer., ε_f = 12.3, d = .6 mm.

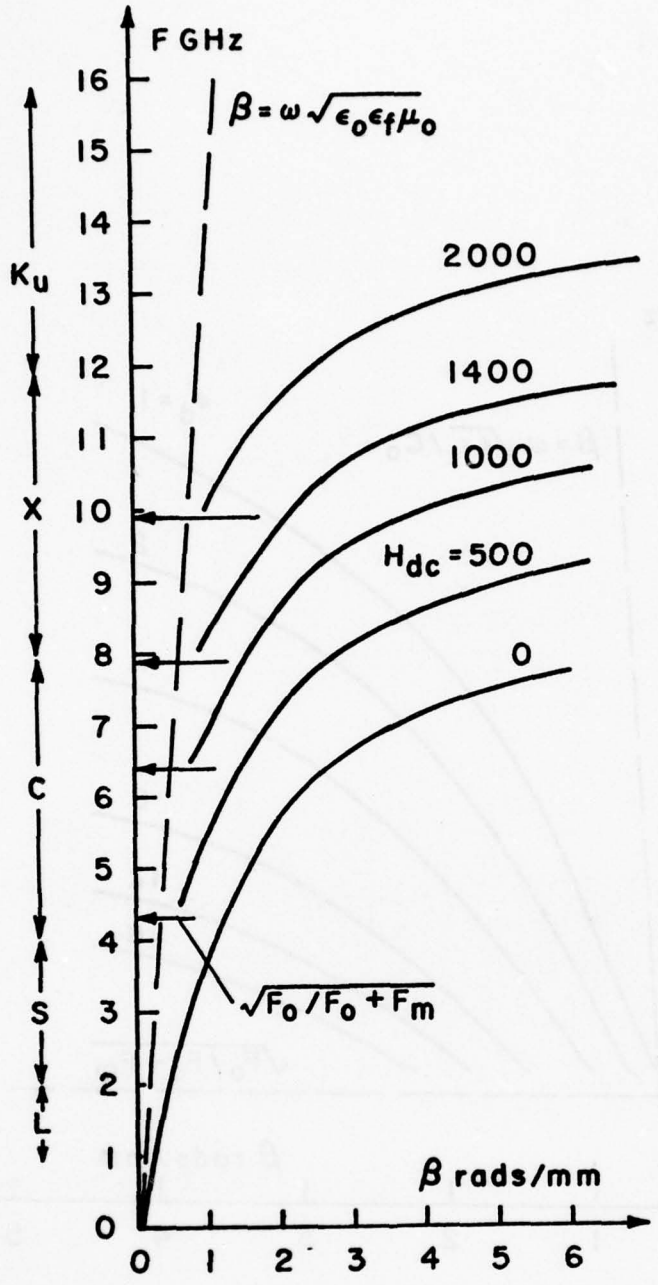

Figure 12 - The dispersion characteristics of the edge-guided mode as a function of the d.c. biasing field. Parameters are: $4\pi M_s$ = 4250 G., ϵ_f = 12.3, ϵ_d = 2.5, d = .6mm.

low field losses at one end and the onset of high dispersion at the upper end.

We next compare the edge-guided and surface modes. Figure 13 shows a sample of the superposition of the edge-guided and surface mode dispersion curves for the three lowest order modes. The surface modes are shown by the broken lines, the edge-guided mode by the solid line. Note that n=1 for the edge-guided mode corresponds to N=0 for the surface mode, and n=2 → N=1, etc.

It is clear that qualitatively there is substantial agreement between the two models even though quantitatively there are substantial differences, particularly for the lowest order mode. It is evident that the edge-guided or peripheral mode and the surface mode are intimately related. That this is so is further confirmed by Figures 14 and 15, where we show a set of dispersion curves for the edge-guided mode and the corresponding impedance characteristics. Comparison with Figures 4 and 9 is invited.

The structure of the edge-guided mode is further illustrated by Figures 16 and 17 where we show the magnitude of the Poynting vector as a function of position and the surface current density in the conducting surfaces. The results are shown in perspective plots where the y=0 plane lies on the conducting ground sheet and the central strip conductor is located at y=.6mm $x > 0$, while for $x < 0$ we have the magnetic wall. It is observed that there is substantial concentration of power particularly for the lower frequency case, at the strip edge where also, of course, the longitudinal component of the current is singular. It is also seen that, as expected, locally within the ferrite the Poynting vector is negatively directed due to the local effective permeability being negative.

The next sequence of figures (18 through 21) gives very similar data for a material with lower saturation magnetization, i.e., 1780 Gauss versus 4250

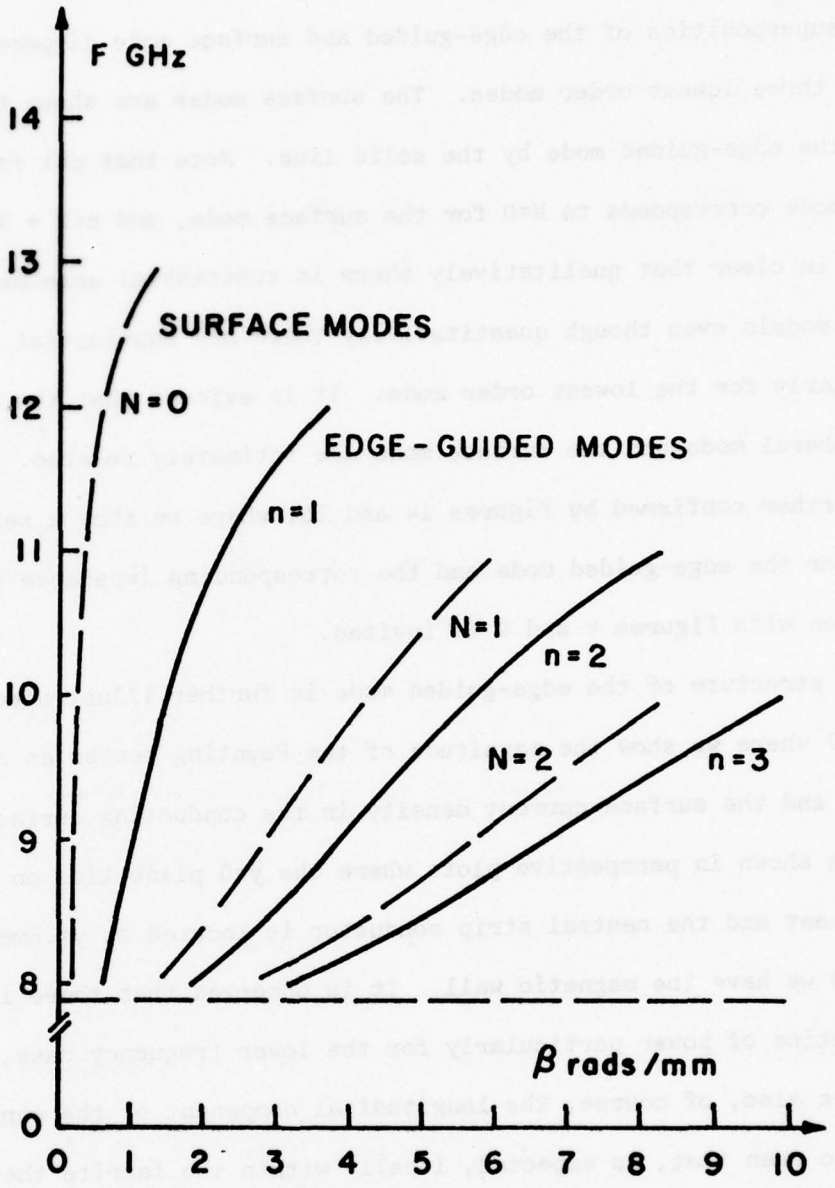

Figure 13 - Comparison of the dispersion characteristics of the surface and the edge guided modes. The parameters are: $4\pi M_s$ = 4250 G., $H_{d.c.}$ = 1400 Oer., ε_f = 12.3, ε_d = 1.0, d = .6mm.

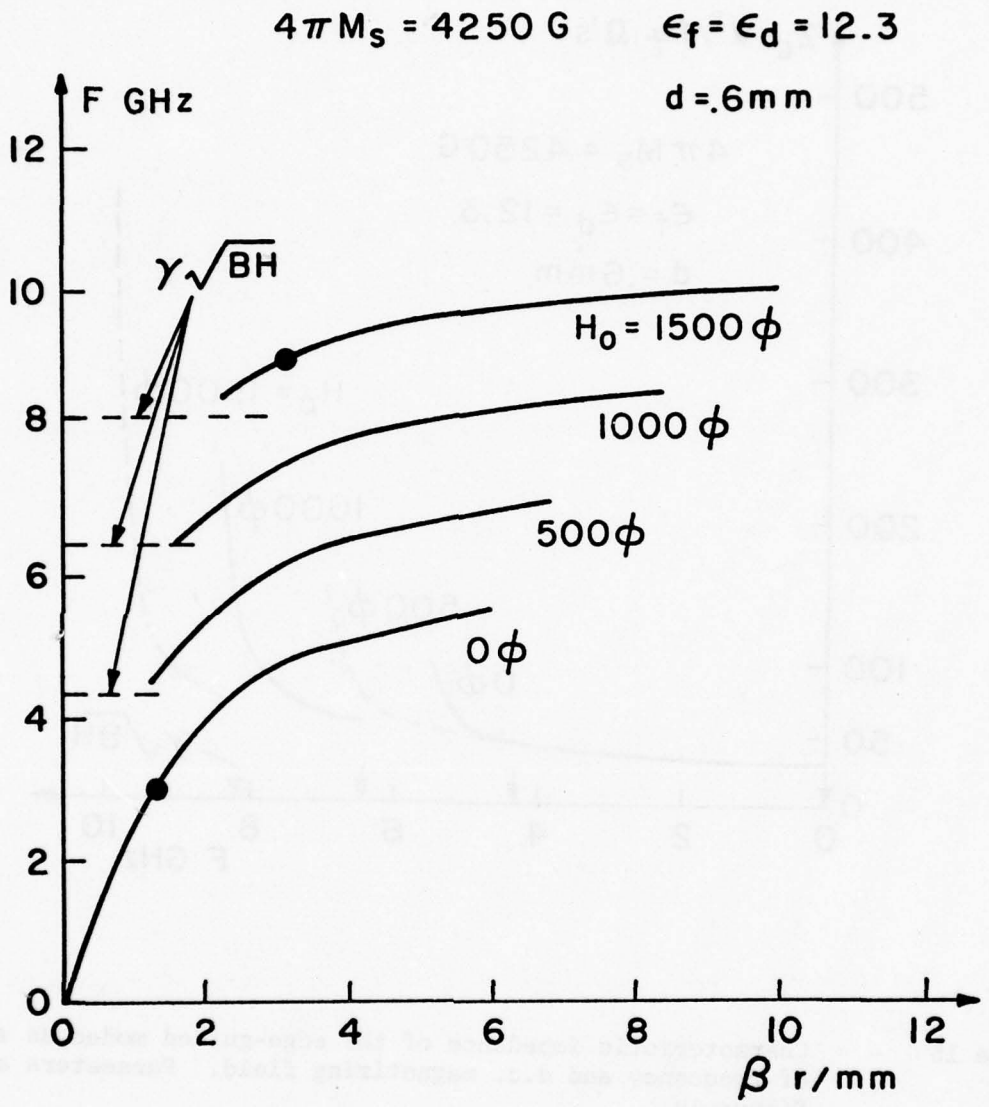

Figure 14 - Dispersion characteristics for the edge-guided mode as a function of the d.c. magnetizing field for $4\pi M_s$ = 4250 G., $\varepsilon_f = \varepsilon_d$ = 12.3, d = .6mm.

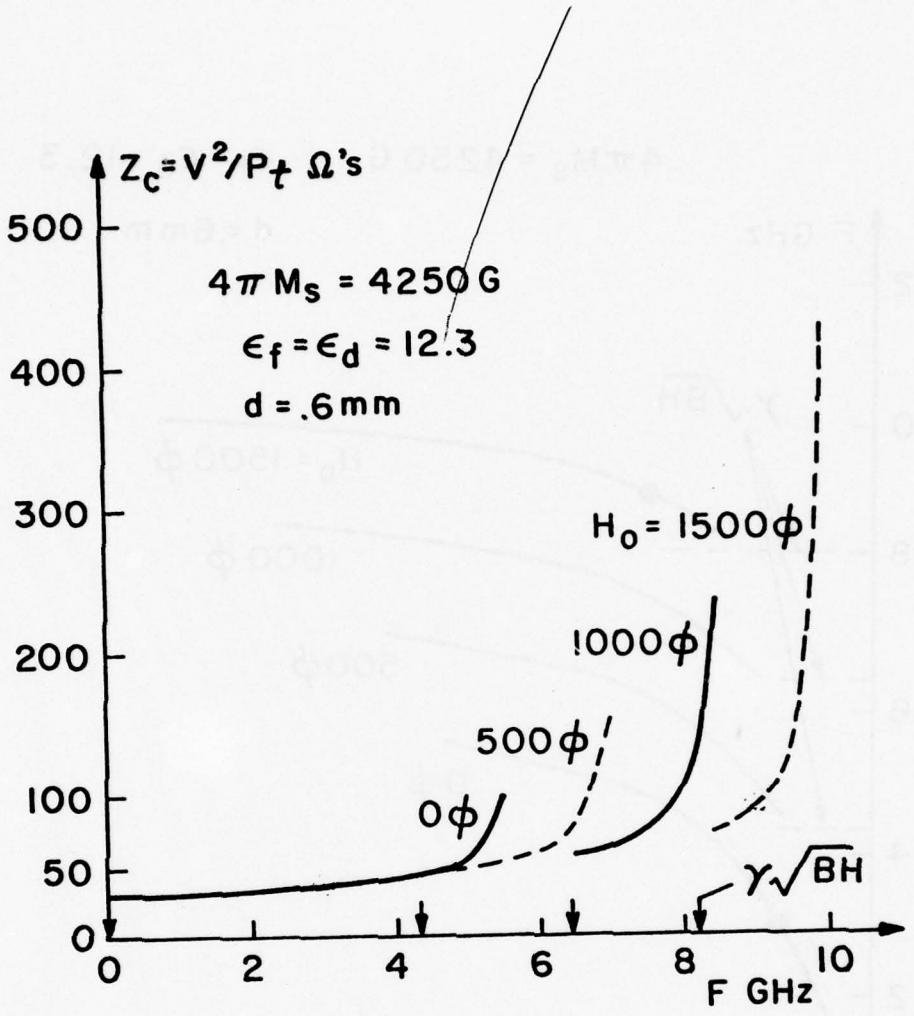

Figure 15 - Characteristic impedance of the edge-guided modes as a function of frequency and d.c. magnetizing field. Parameters are for Figure 14.

$4\pi M_s = 4250\ G \quad H_o = 0\phi \quad \epsilon_f = \epsilon_d = 12.3 \quad d = .6mm$

$F = 3.00\ GHz \quad \beta = 1.3017\ r/mm$

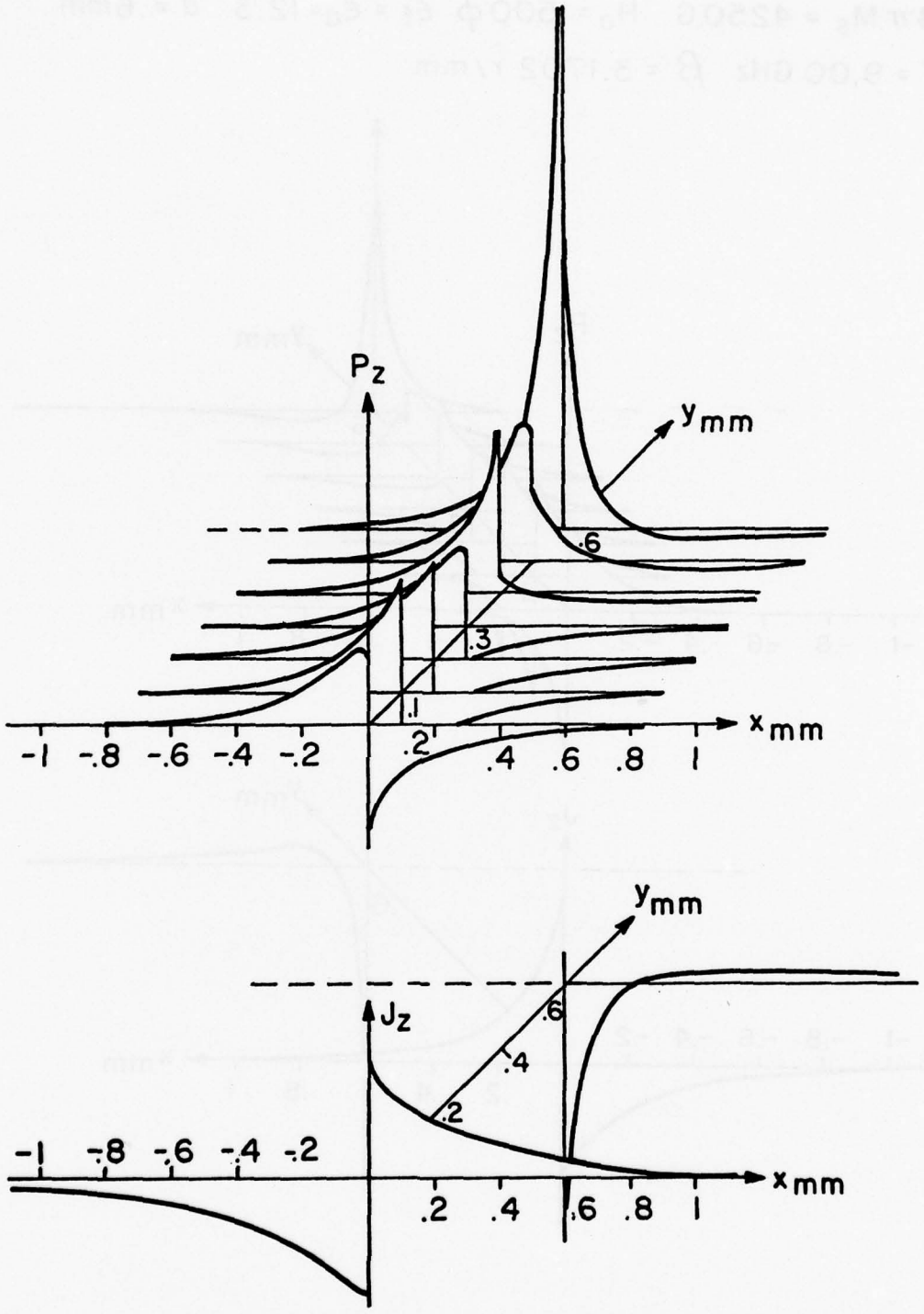

Figure 16 - The poynting vector axial component as a function of position in the edge-guide transverse section and the axial components of the surface currents induced on the conducting planes for f = 3 GHz. (see Fig. 14)

$4\pi M_s = 4250\,G \quad H_0 = 1500\,\phi \quad \epsilon_f = \epsilon_d = 12.3 \quad d = .6mm$

$F = 9.00\,GHz \quad \beta = 3.1702\ r/mm$

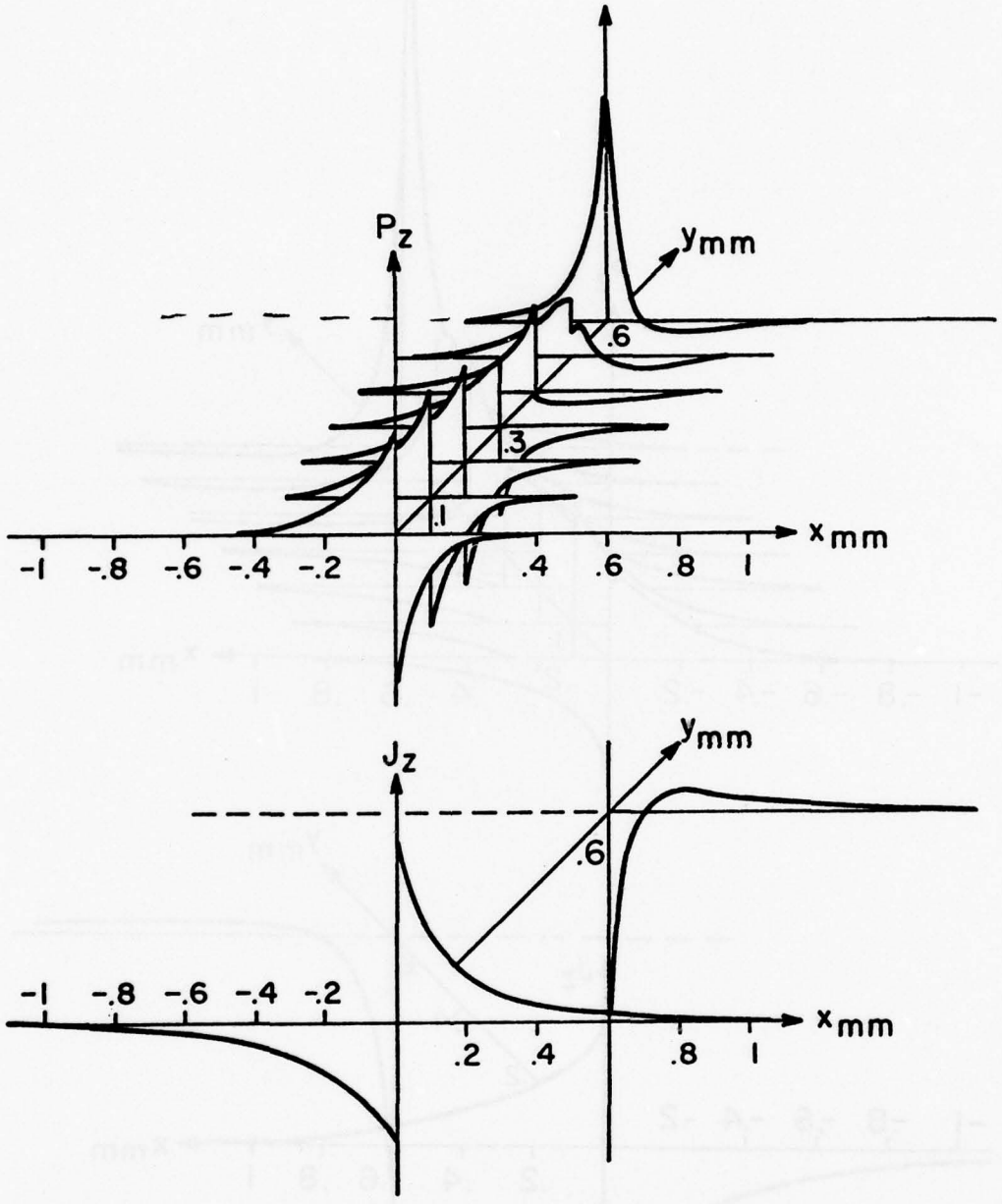

Figure 17 - See Figure 16 but for a frequency of 9 GHz.

$4\pi M_s = 1780\,G \quad H_o = 220\phi \quad \epsilon_f = \epsilon_d = 14.5 \quad d = .6mm$

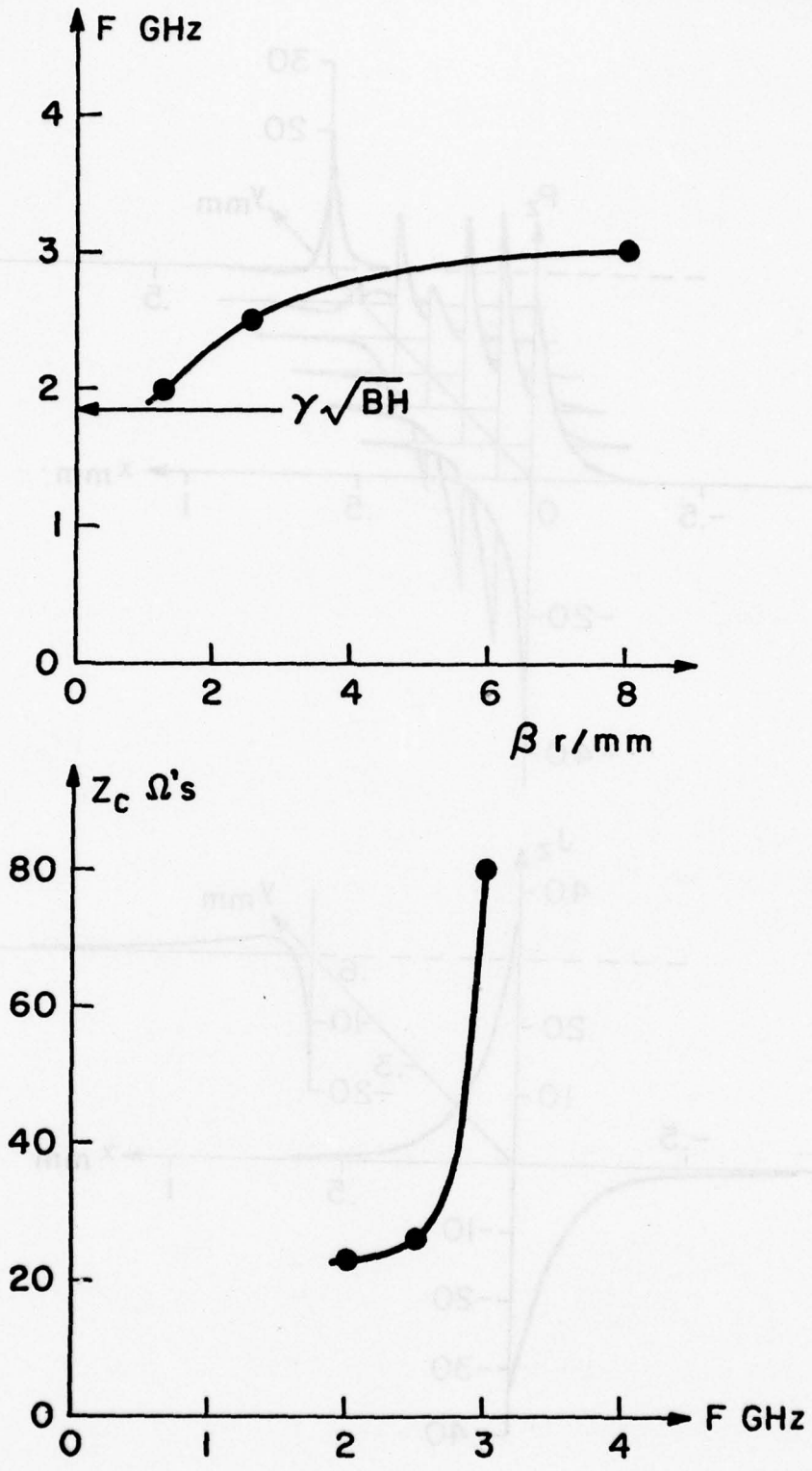

Figure 18 - The dispersion and impedance characteristics for the edge-guided mode when $4\pi M_s$ = 1780 G., H_o = 220ϕ, $\epsilon_f = \epsilon_d$ = 14.5 and d = .6mm.

$4\pi M_s = 1780G \quad H_o = 220\phi \quad \epsilon_f = \epsilon_d = 14.5 \quad d = .6mm$

$F = 3.00GHz \quad \beta = 8.0022\, r/mm$

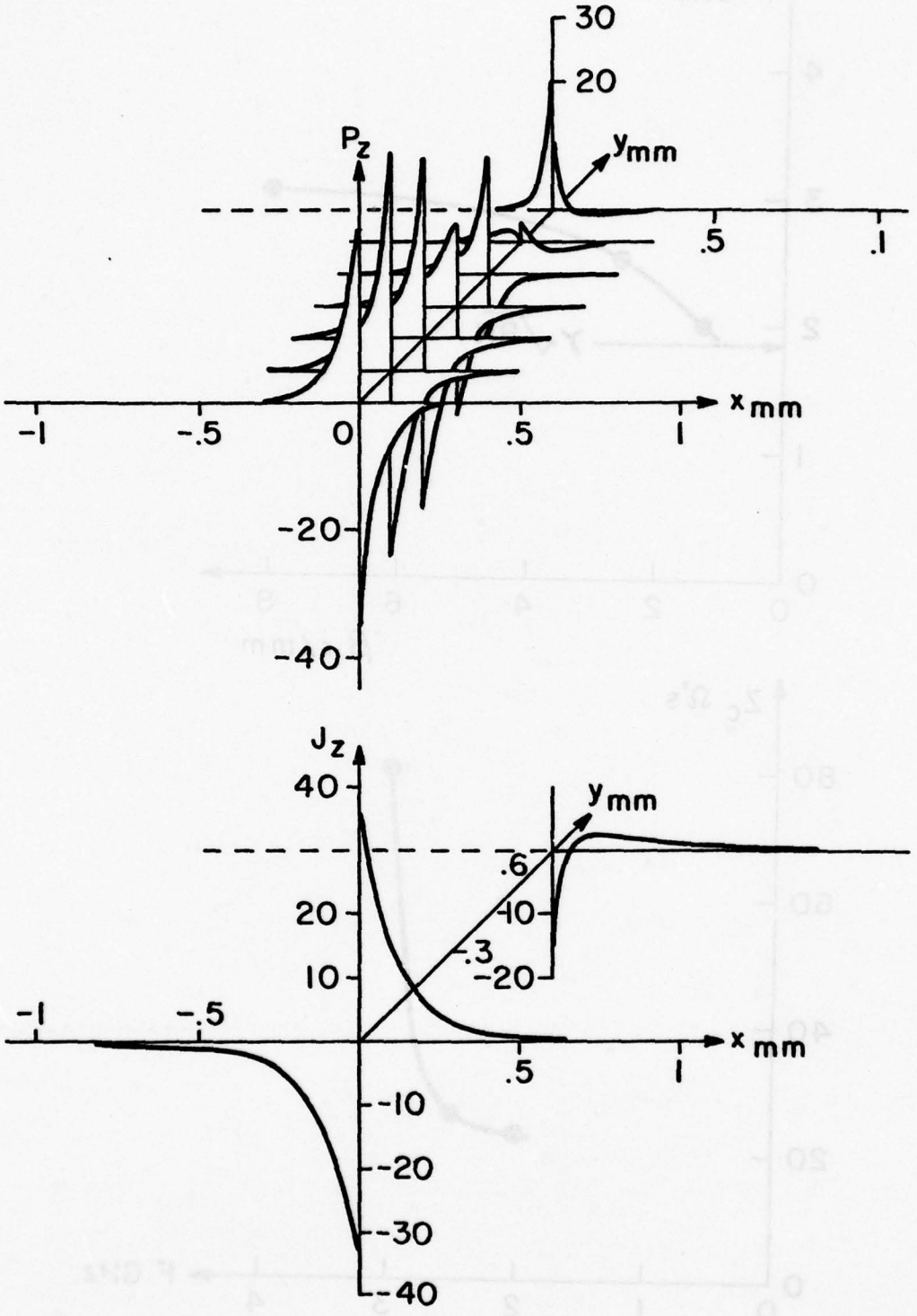

Figure 19 - See Figure 16 but for the parameters of Figure 18 and f = 3 GHz.

$4\pi M_s = 1780\,G \quad H_o = 220\,\phi \quad \epsilon_f = \epsilon_d = 14.5 \quad d = .6\,mm$

$F = 2.50\,GHz \quad \beta = 2.5214\ r/mm$

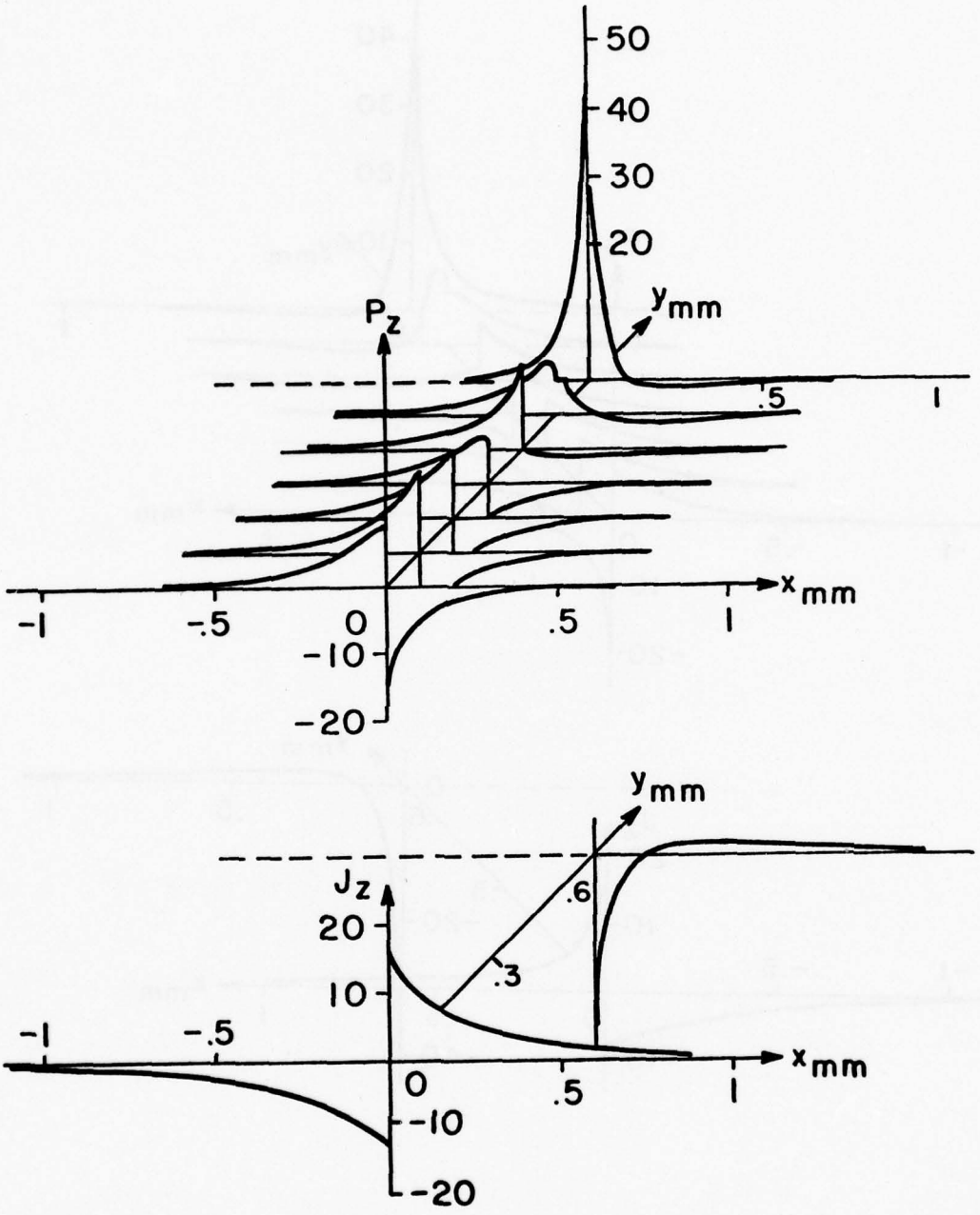

Figure 20 - See Figure 16 and f = 2.5 GHz.

$4\pi M_s = 1780G \quad H_0 = 220\phi \quad \epsilon_f = \epsilon_d = 14.5 \quad d = .6mm$

$F = 2.00\,GHz \quad \beta = 1.2859\ r/mm$

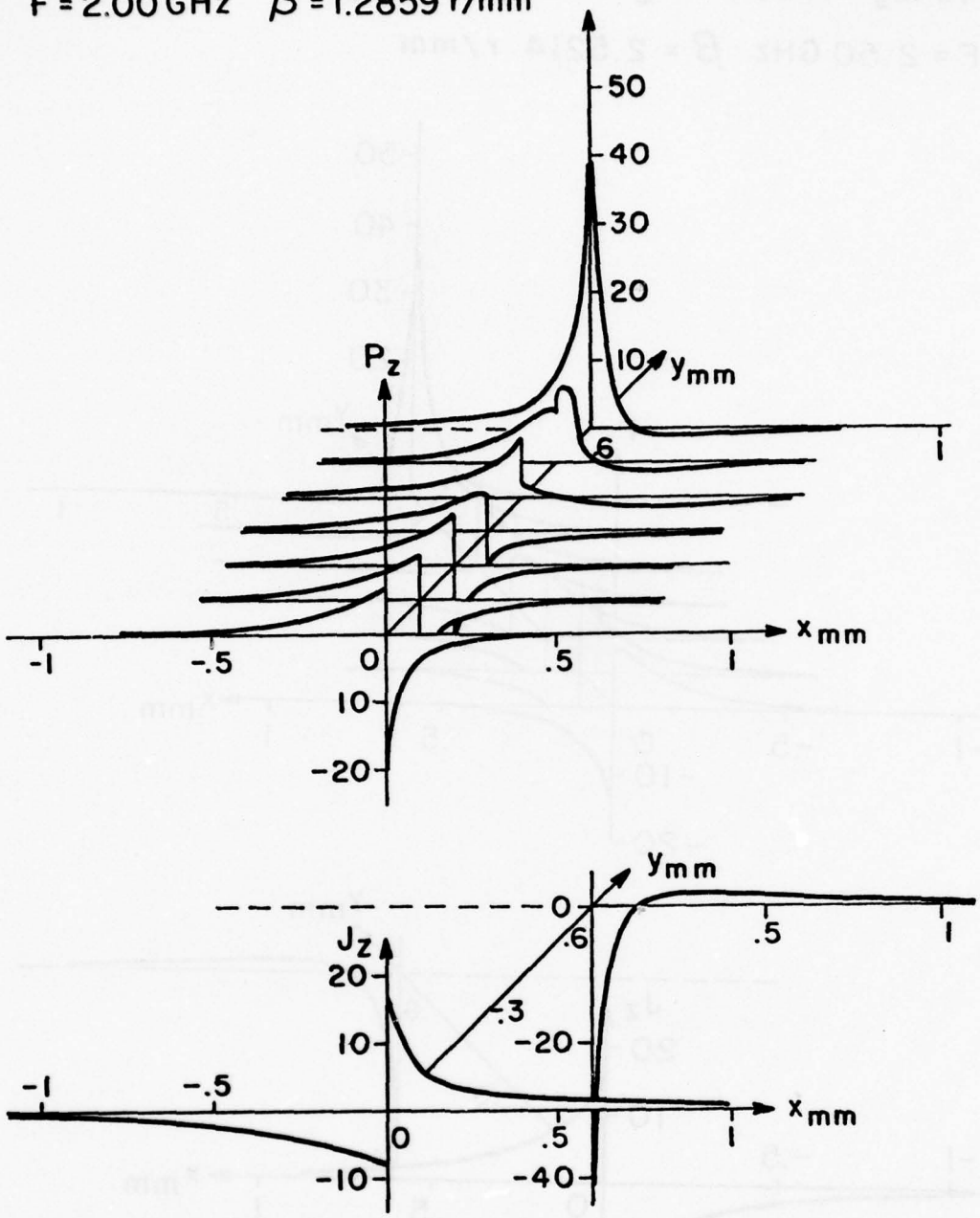

Figure 21 - See Figure 16 and f = 2.0 GHz.

Gauss. We observe that the previous remarks apply equally.

To complete this section of the report we present some results obtained for the model field component structure both to justify further the sufficiency of the approximate numerical approach in the determinant truncation and in comparing the surface and edge-guided modal structure.

Figures 22 through 24 show the field components at the ferrite-dielectric interface. The dashed lines denote the components evaluated at $x = 0^+$ while the solid lines give the components for $x = 0^-$. All three figures are for the case where we used eight coefficients in the series expansions i.e., eight TE and eight TM 'modes' on the dielectric side of the boundary and eight terms in each of the two series required to represent the fields on the ferrite side (see page), thus yielding a sixteen by sixteen trunhated determinant. Each of the entries in the determinant was summed to twenty terms which yielded, as was mentioned earlier, a worst accuracy of 5% in the propagation factor.

Figure 22 presents, for a typical case, the four tangential components which should be continuous across the interface. Agreement is more than adequate when we realize that the primary field components with which we work are e_y and b_y and that the e_z and h_z components are obtained in terms of e_y and h_y. Figures 23 and 24 give further sample results but for a material having high saturation magnetization. Also, in these latter cases, all six field components are given for a low frequency as well as high frequency situation, i.e., 3 and 9 GHz, respectively. Figures 25 and 26 give some further results on the structure of the higher order edge-guided modes. These data pertain to Fig. 13 where we showed the higher order edge-guided and surface modes. Figure 25 gives the fields on both sides of the ferrite-dielectric interface while for the first higher order mode, the dashed curves indicate the structure of the corresponding surface mode. Figure 26 gives the behavior of the field transverse

$4\pi M_s = 1780\,G \quad H_o = 220\,\phi \quad \epsilon_f = \epsilon_d = 14.5 \quad d = .6mm$

$F = 2.50\,GHz \quad \beta = 2.5214\ r/mm$

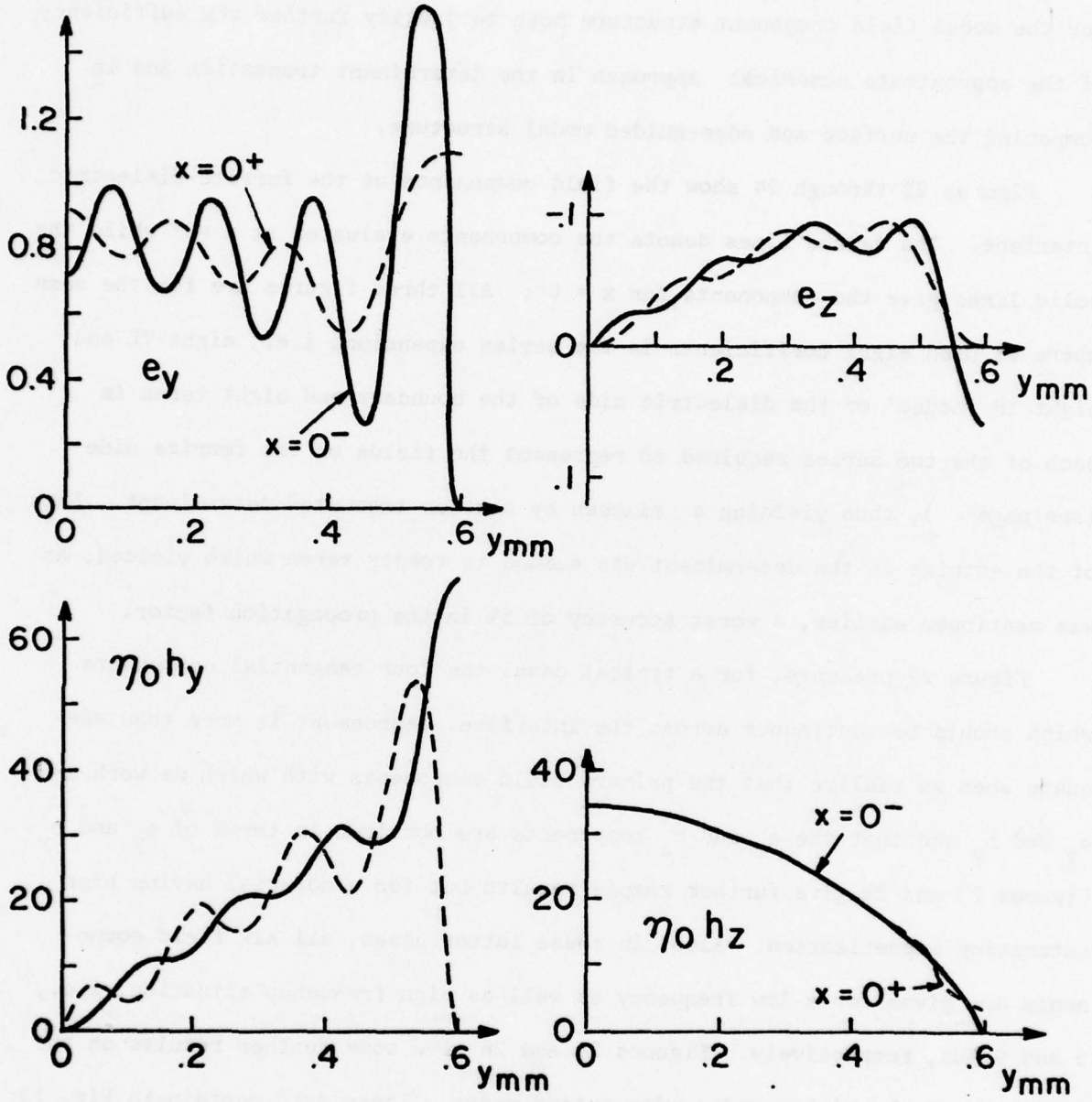

Figure 22 - Field structure of the lowest order edge-guided mode. Components of the field tangential to the ferrite-dielectric interface shown on the interface for $4\pi M_s$ = 1780 G, H_o = 220ϕ, $\epsilon_f = \epsilon_d$ = 14.5, d = .6mm, f = 2.5 GHz.

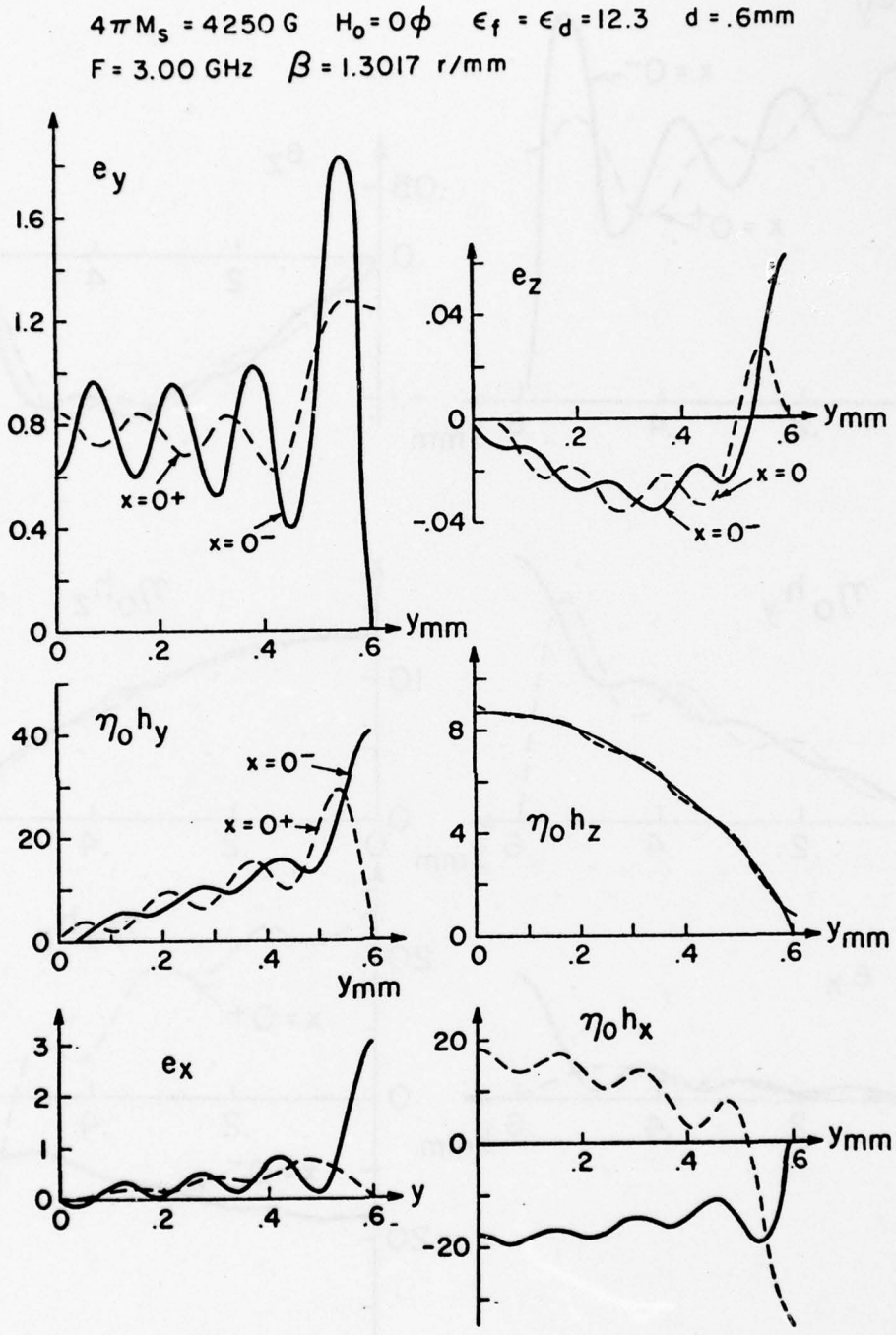

Figure 23 - Field structure of the lowest order edge guided on the ferrite dielectric interface. Parameters as for Figure 14, frequency = 3 GHz, $H_o = 0$.

$4\pi M_s = 4250\,G \quad H_o = 1500\,\phi \quad \epsilon_f = \epsilon_d = 12.3 \quad d = .6mm$

$F = 9.00\,GHz \quad \beta = 3.1702\ r/mm$

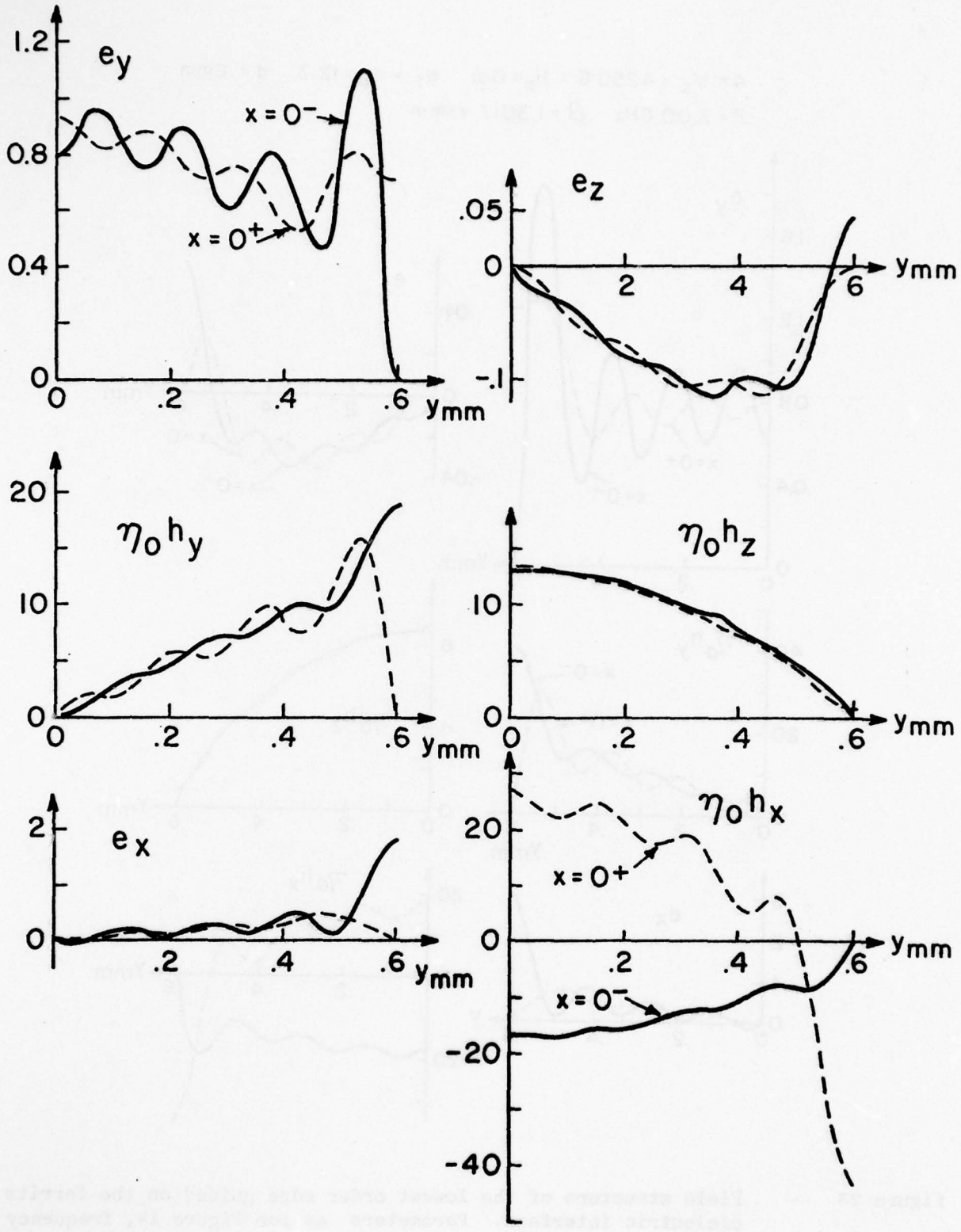

Figure 24 - See Figure 23 but with f = 9 GHz, H_o = 1500 .

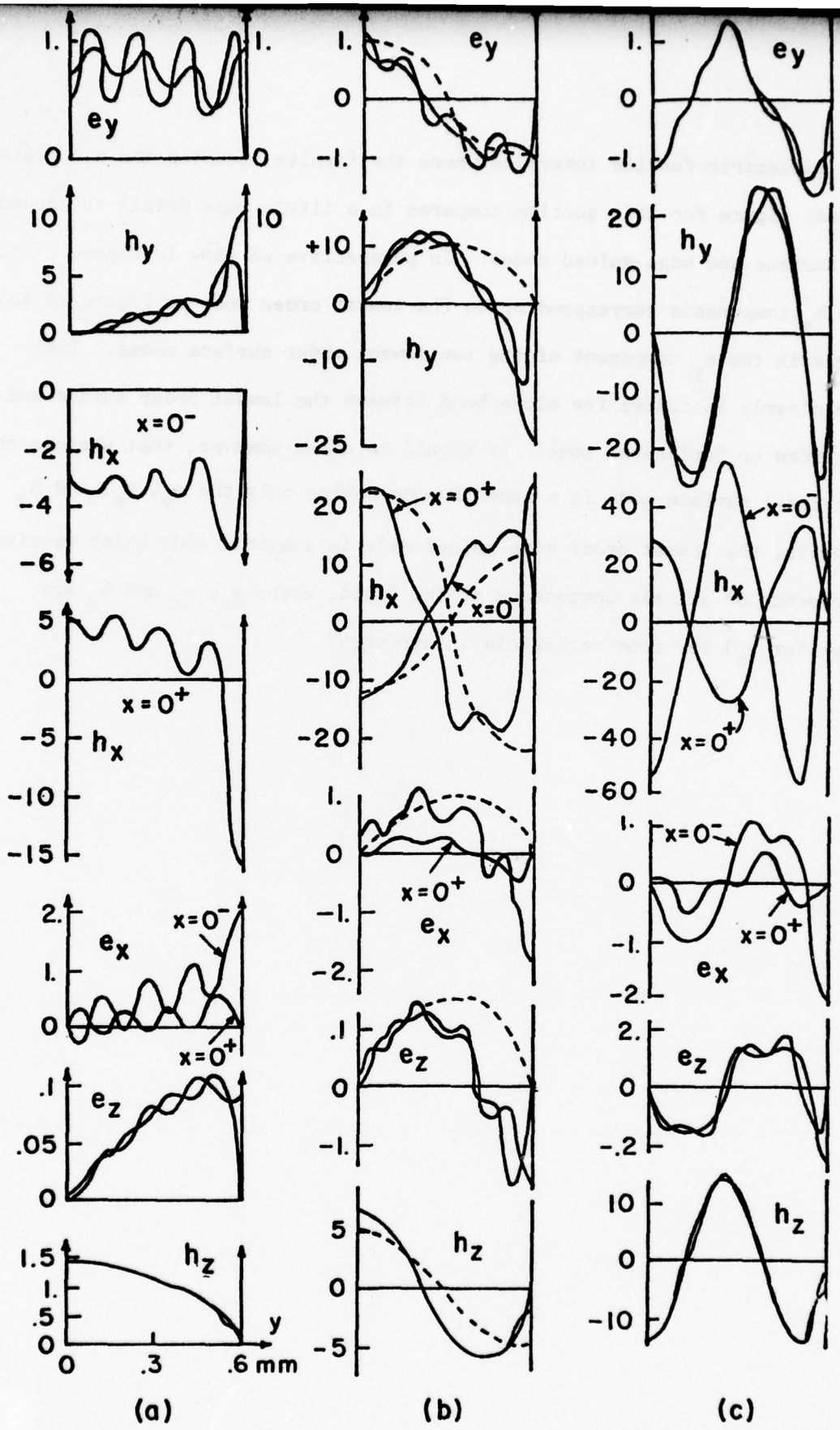

Figure 25 - Field structure of the three lowest order edge-guided modes on the ferrite-dielectric interface x = 0, y = 0→d. Parameters are: F = 9 GHz, $4\pi M_s$ = 4250 G., $H_{d.c.}$ = 1400 Oer., ε_f = 12.3, ε_d = 1.0 d = .6mm. a)β = 1.068 r/mm., b)β = 3.847 r/mm., c) β = 6.692 r/mm.

to the dielectric-ferrite interface where the ferrite occupies the x>0 region. The final figure for this section compares in a little more detail the lowest order surface and edge-guided modes. In perspective we show in Figure 27 the e_y and h_y components corresponding to the lowest order mode of Figure 25 together with the e_y component of the two lowest order surface modes. This figure clearly indicates the close bond between the lowest order suface and edge-guided or peripheral mode. It should be noted however, that whereas the lowest order surface mode is a pure TE mode having only the e_y, h_x, and h_z components, the lowest order edge-guided mode is a hybrid mode which requires the presence of all six components of the field, where e_x, e_z and h_y are (except for e_z) far from negligible in strength.

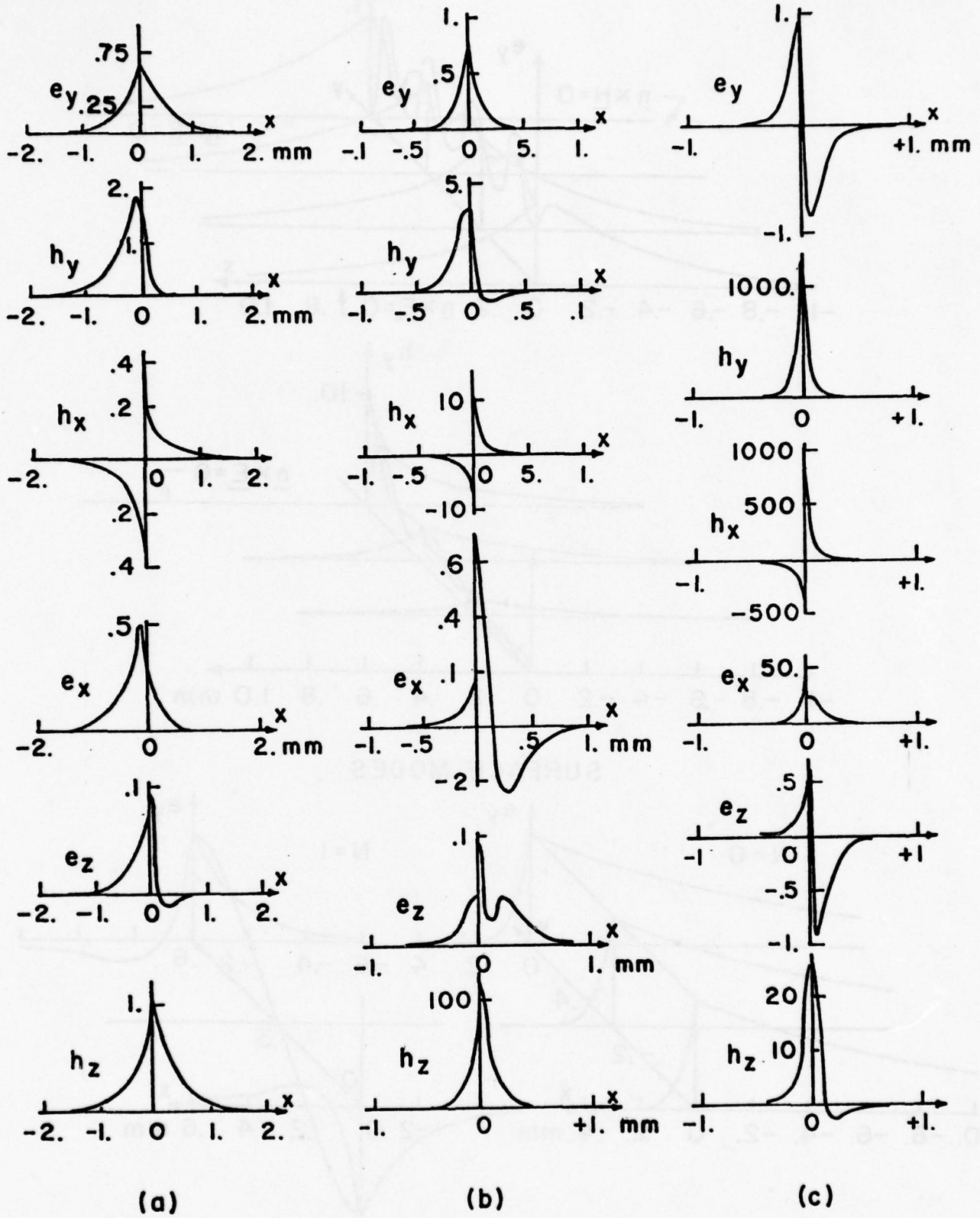

Figure 26 - Field Structure of the three lowest order edge-guided modes as a function of the transverse coordinate x. Data as for Fig. 25.

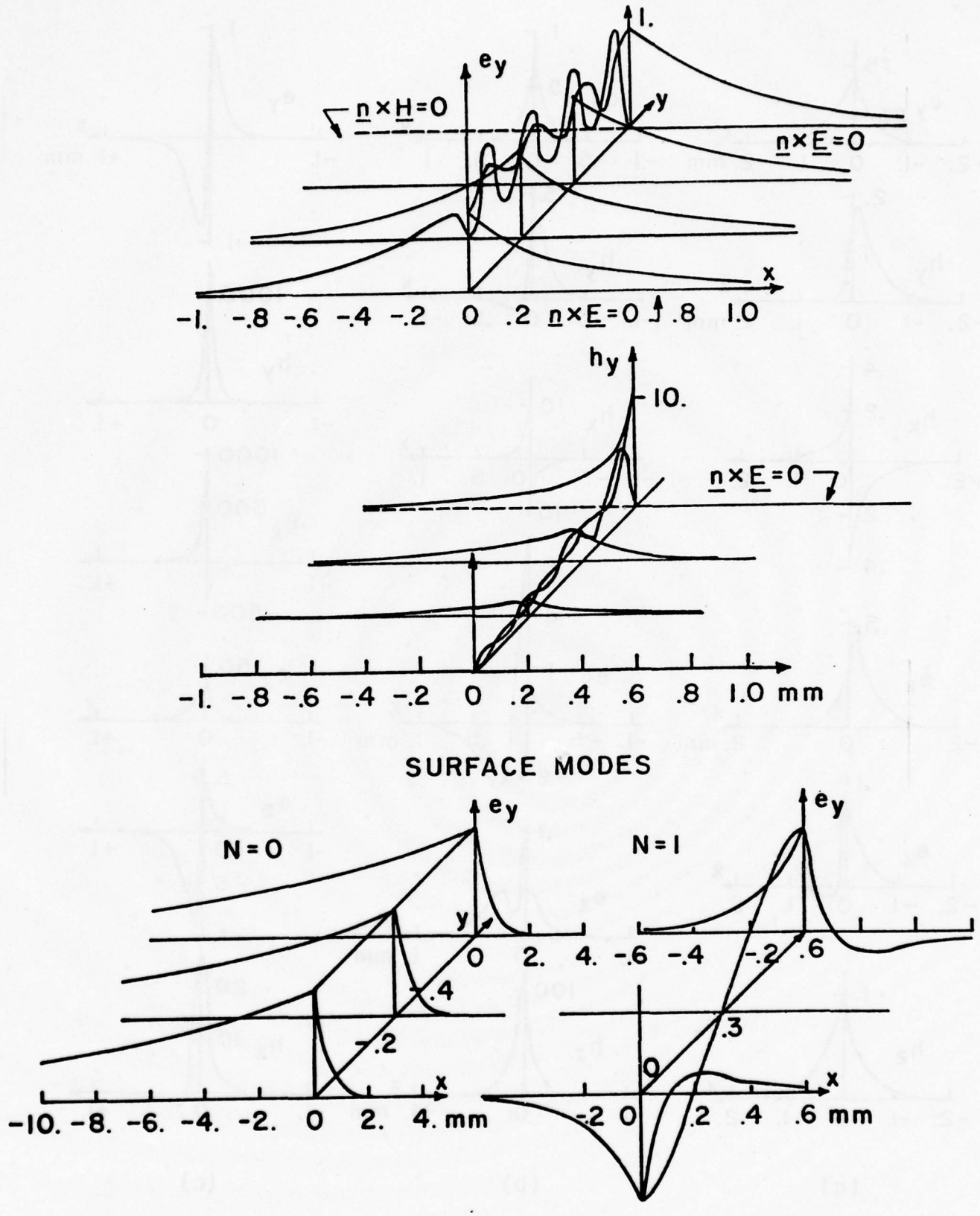

Figure 27 - Field structure of the lowest order edge-guided and surface modes compared. Data as for Figs. 25, 3, 5. f = 9.0 GHz.

II (d) Conclusions:

Results have been presented which were obtained from rigorous solutions of waveguiding geometries which exhibit surface wave and edge-guided wave phenomena. These results clearly establish the unidirectional nonreciprocal nature of the modes. With the groundplane of the guiding structure located at the $y = 0$ surface and the ferrite slab occupying the $x > 0$ region we observe that these modes adhere to the dielectric-ferrite interface and the edge only for propagation in the positive z direction for the d.c. magnetic field biasing in the positive y direction, i.e., we have a field displacement to the left when viewed in the direction of propagation. Secondly, the modes only exist for that range of frequencies for which the effective permeability is negative. The resultant band limited bahavior is further limited drastically by the higher dispersive behavior of these modes as the frequency increases. For example, for a saturation magnetization of 4250 Gauss and a d.c. magnetizing field of 500 Oersteds the effective permeability is negative over the range 4.3 → 13.3 GHz. However, the actual bandwidth of the edge-guided mode (Fig. 14) is only of the order of 2 GHz and does not nearly match the 9 GHz negative permeability range. Thirdly, it was concluded that there is a direct relationship between the surface modes and the edge-guided modes for the model structures investigated here. This was established on the basis of similarity in the dispersion characteristics (ω-β diagrams) and the basic modal field structures.

The final conclusion reached was that it was unlikely that devices purportedly using the edge-guided mode in fact did so.

This conclusion led to the next part of the study which considers a more general geometry and one which more nearly models the ferrite width stripline geometries employed in isolators and phase shifters.

III The Stripline Modal Spectrum

III (a) Introduction

Our earlier studies described in part II of this report and also discussed at several conferences[27,30,34,35], investigated the edge-guided or peripheral mode and established the bandwidth to be expected if device operation was restricted to utilization of these modes. In addition, the relationship between the surface modes and the edge-guided modes on appropriate canonical structures was investigated. It was concluded that the edge-guided mode is a perturbed surface mode, and exists only in that range of frequencies where the effective permeability is negative. Furthermore, the edge-guided mode adheres rather tightly to the edge of the stripline and tends to be highly dispersive.

From experimental work by deSantis[16,21], Rosenbaum[23] and Courtois[19] and other workers it has become evident that devices which were presumed to depend on the edge-guided mode in fact continued to operate beyond those frequencies where the edge-guided mode could exist.

It therefore became necessary to extend the analysis to structures which more closely model the ferrite loaded stripline. The geometries of Fig. 28 were therefore considered. Fig. 28(c) shows the transverse section of the shielded microstrip line which is one of the objectives of our study. A slight modification to this figure gives the equally important homogeneously or inhomogeneously ferrite loaded stripline. The extensive and difficult analysis which will be required for a rigorous investigation of the full modal characteristics of such transmission lines forces us to consider the somewhat simpler alternative of Figure 28(b), the inhomogeneously ferrite loaded stripline. What is required here is an extension of the analysis applied to the geometry of Fig. 1(c). The finite width of the ferrite and conductor presents us with a three region problem.

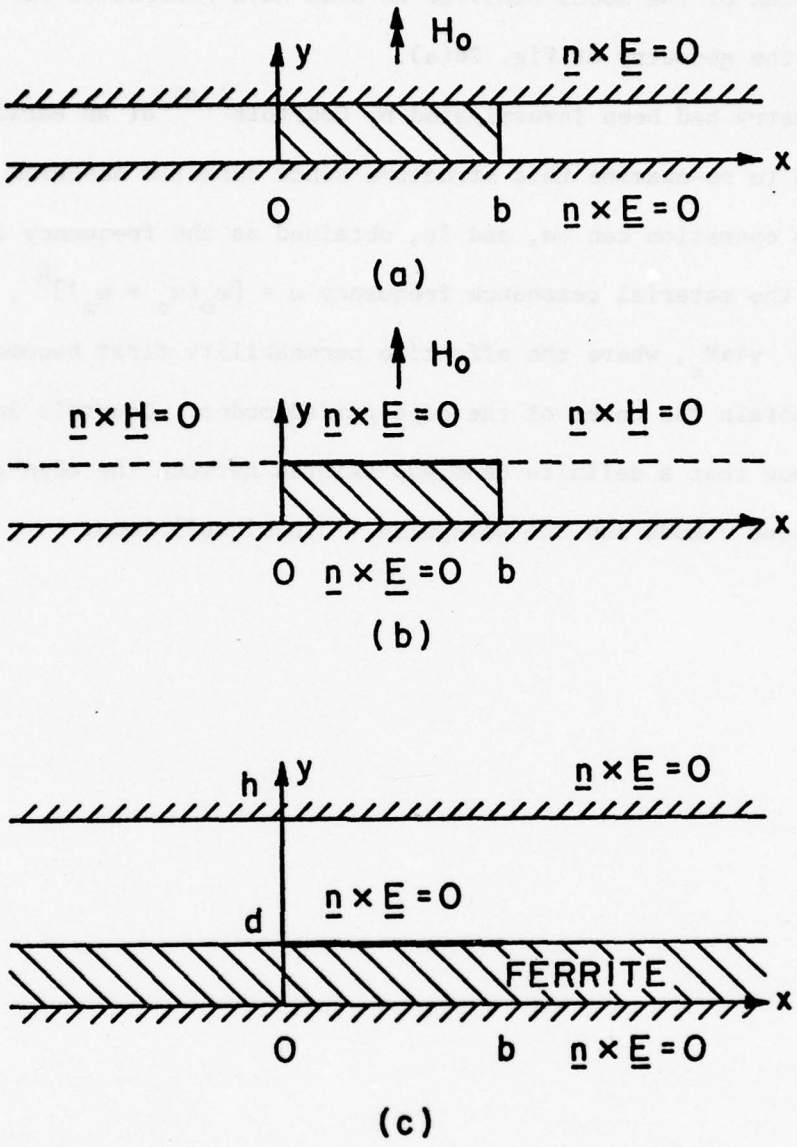

Figure 28 - Canonical stripline geometries for ferrite loaded components.

Having seen earlier that the semi-infinite ferrite slab between parallel, perfectly conducting planes gave a good qualitative if not very accurate quantitative indication of the modal behavior we also have restricted our first consideration to the geometry of Fig. 28(a).

This geometry had been investigated by Courtois[19] at an earlier date. It was decided to re-examine this structure since deSantis observed that continuous device operation can be, and is, obtained as the frequency is increased starting from the material resonance frequency $\omega = [\omega_o(\omega_o + \omega_m)]^{\frac{1}{2}}$, $\omega_o = \partial H_{dc}$, $\omega_m = \gamma 4\pi M_s$, where the effective permeability first becomes negative and where we obtain the onset of the edge-guided modes. Courtois in his results appeared to show that a definite band gap existed between the edge-guided ('magnetostatique') mode and the waveguide ('dynamique') mode.

III (b) Theory:

The theoretical approach taken parallels that of section II(b) for the two region problem. The following restrictions were observed. First, the ferrite and dielectric media were presumed lossless and no conductor losses were taken into account. Secondly, only the lowest order modes were considered, i.e., no variation w.r.t the y-coordinate ($\partial/\partial y = 0$). The only mode types allowed were those which were restricted to the vicinity of the ferrite strip. Thus the transverse dependence for x positive was taken of the form $\exp(-|\alpha|x)$ for $x>0$ and $\exp(+|\alpha|x)$ for $x < 0$. Completing the expressions for the various field components and meeting the required boundary conditions yields a transcendental form for our dispersion relation,

$$\tan \alpha_f b' = \frac{-2\alpha_d \alpha_f r}{\beta'^2(\mu_f + \frac{1}{1+\chi}) - 1 - \nu^2 \mu_f}$$

where

$$r = \sqrt{\varepsilon_d/\varepsilon_f}$$

$$\alpha_f^2 = \beta'^2 - \mu_f$$

$$\alpha_f^2 = (\beta'^2/r^2) - 1$$

$$\mu_f = (1+\chi) - \kappa^2/(1+\chi)$$

$$\beta' = \beta/k_f$$

$$k_f = \omega\sqrt{\mu_o \varepsilon_f \varepsilon_o} = \omega\sqrt{\varepsilon_f/c_o}$$

$$b' = k_f b$$

and b is the width of the ferrite strip.

The expressions for the field components in the three regions are cumbersome and will not be given here.

Note that α_f is not restricted to being real but can, and does, become purely imaginary thus leading to a trigonometric rather than exponential transverse field dependence within the ferrite.

III (c) Results

The first results obtained are shown in Figure 29. Calculated were the dispersion curves for a ferrite strip of width 5 mm. The ferrite saturation magnetization was taken to be 1760 Gauss, the d.c. magnetic bias was 200 Oersted, the permittivity of the ferrite was 15 and the regions exterior to the ferrite were taken to be free space. The horizontal broken lines initiate the region over which the effective permeability of the ferrite is negative while the dashed curves give the lowest and first higher order mode for the equivalent isotropic case.

We observe that for frequencies below the material resonance we obtain the volume modes which were also obtained by Courtois[19]. Within the region where the permeability is negative we obtain the surface mode which was described in detail in section II of this report. Restricted to the sector which is contained between lines whose slopes are the velocity of plane waves in the dielectric medium and in a dielectric medium with the same permittivity as the ferrite and free space permeability, are the zero cut-off quasi-TEM mode as well as the next two higher order mode. We note the perturbation of the two lowest order modes from their isotropic counterparts. Also shown are the transverse distributions of the e_y component of the field. It was of considerable interest to observe that the broad band zero-cut off quasi-TEM mode displays a strong field displacement effect over a range of frequencies which substantially exceeded the region where μ_f is negative.

A more detailed investigation was then made for the case where the ferrite strip width was increased to 10. mm. (The results are shown in Fig. 30.) Here we show the two lowest order isotropic modes in light solid line while the various limits of the regions where different modes may occur are shown in dashed lines.

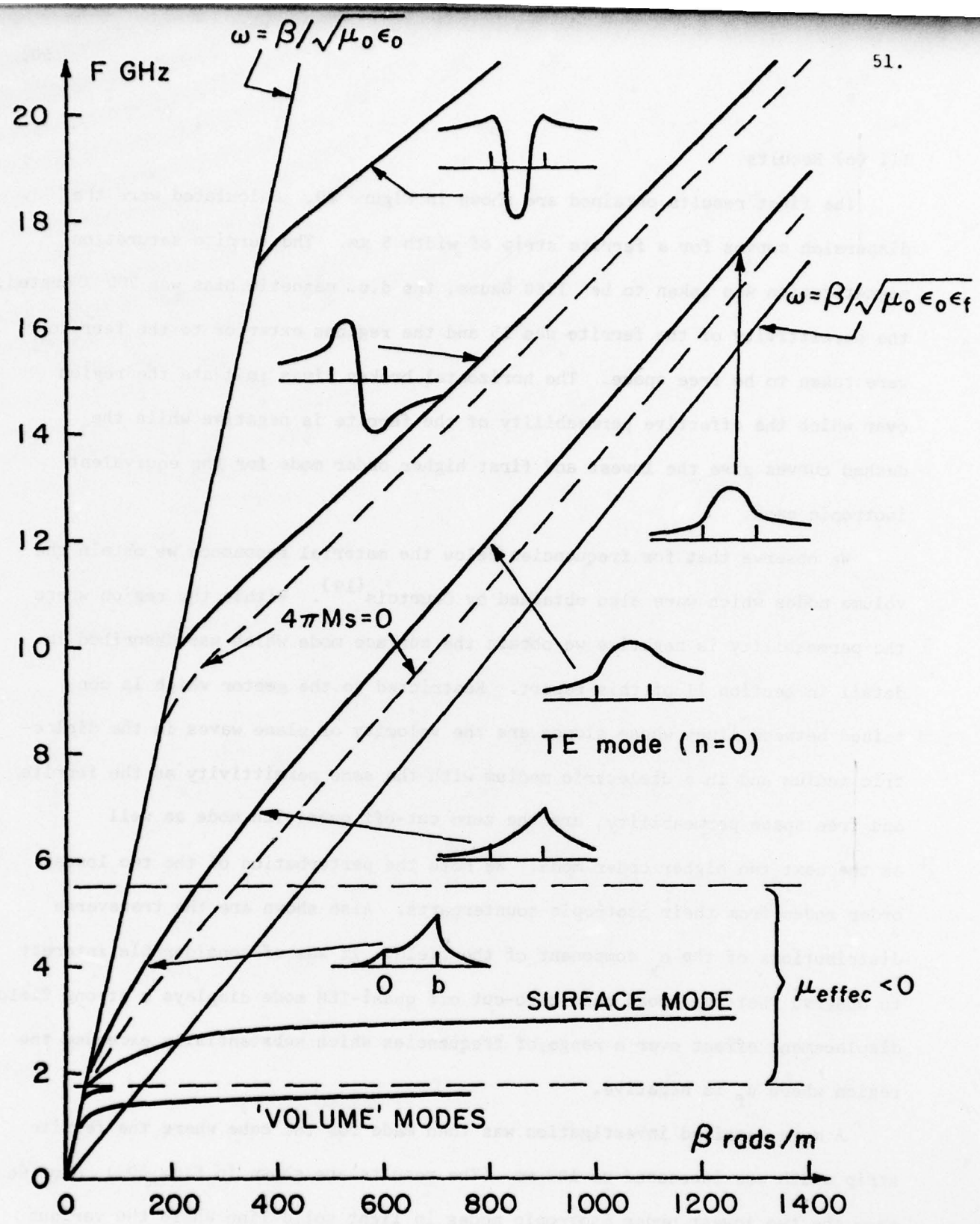

Figure 29 - Dispersion characteristics and transverse electric field distributions for the lowest order mode ($\partial/\partial y = 0$) for the canonical stripline structure of Fig. 26(a). $4\pi M_s$ = 1760 G, H_o = 200ϕ, ϵ_f = 15, ϵ_d = 1.0, b = 5 mm. Dashed curves gives the corresponding isotropic case $4\pi M_s = 0$.

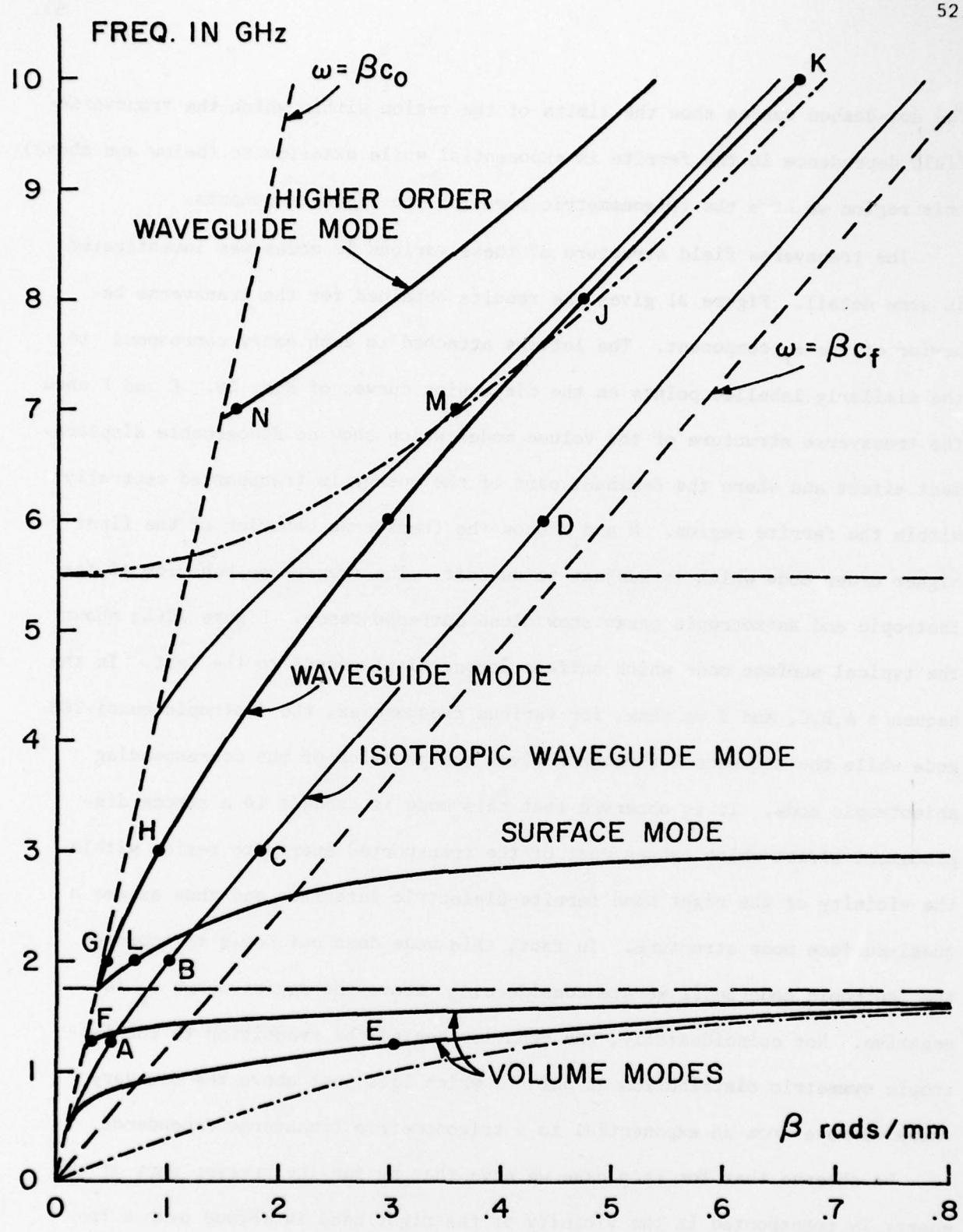

Figure 30 - See Figure 27 but with ferrite width b increased to 10 mm. Isotropic results shown in light solid line. (See text for detailed explanation.)

The dot-dashed curves show the limits of the region within which the transverse field dependence in the ferrite is exponential while exterior to (below and above) this region we have the trigonometric form for the field components.

The transverse field structure of these various TE modes was investigated in some detail. Figure 31 gives the results obtained for the transverse behavior of the e_y component. The letters attached to each entry correspond to the similarly labelled points on the dispersion curves of Fig. 30. E and F show the transverse structure of the volume modes which show no discernable displacement effect and where the dominant part of the energy is transported centrally within the ferrite region. M and N show the transverse behavior of the first higher order mode which is subject to cut-off. The transverse behavior of the isotropic and anisotropic cases show close correspondence. Figure 30(L) shows the typical surface mode which suffers strong displacement to the left. In the sequence A,B,C, and D we show, for various frequencies, the isotropic quasi-TEM mode while the sequence G through K gives the behavior of the corresponding anisotropic mode. It is observed that this mode is subject to a strong displacement effect which causes most of the transported energy to reside within the vicinity of the right hand ferrite-dielectric interface and thus assume a quasi-surface mode structure. In fact, this mode does not begin to approach the isotropic mode until we are considerably above the region where μ_f is negative. Not coincidentally, the behavior begins the transition to the isotropic symmetric distribution at point J which lies just above the boundary where we move from an exponential to a trigonometric transverse dependence.

We observe that for this case we have that by far the greater part of the energy is transported in the vicinity of the right hand interface over a frequency range from about 2 to 8 GHz, i.e., a two octave bandwidth. The bandwidth

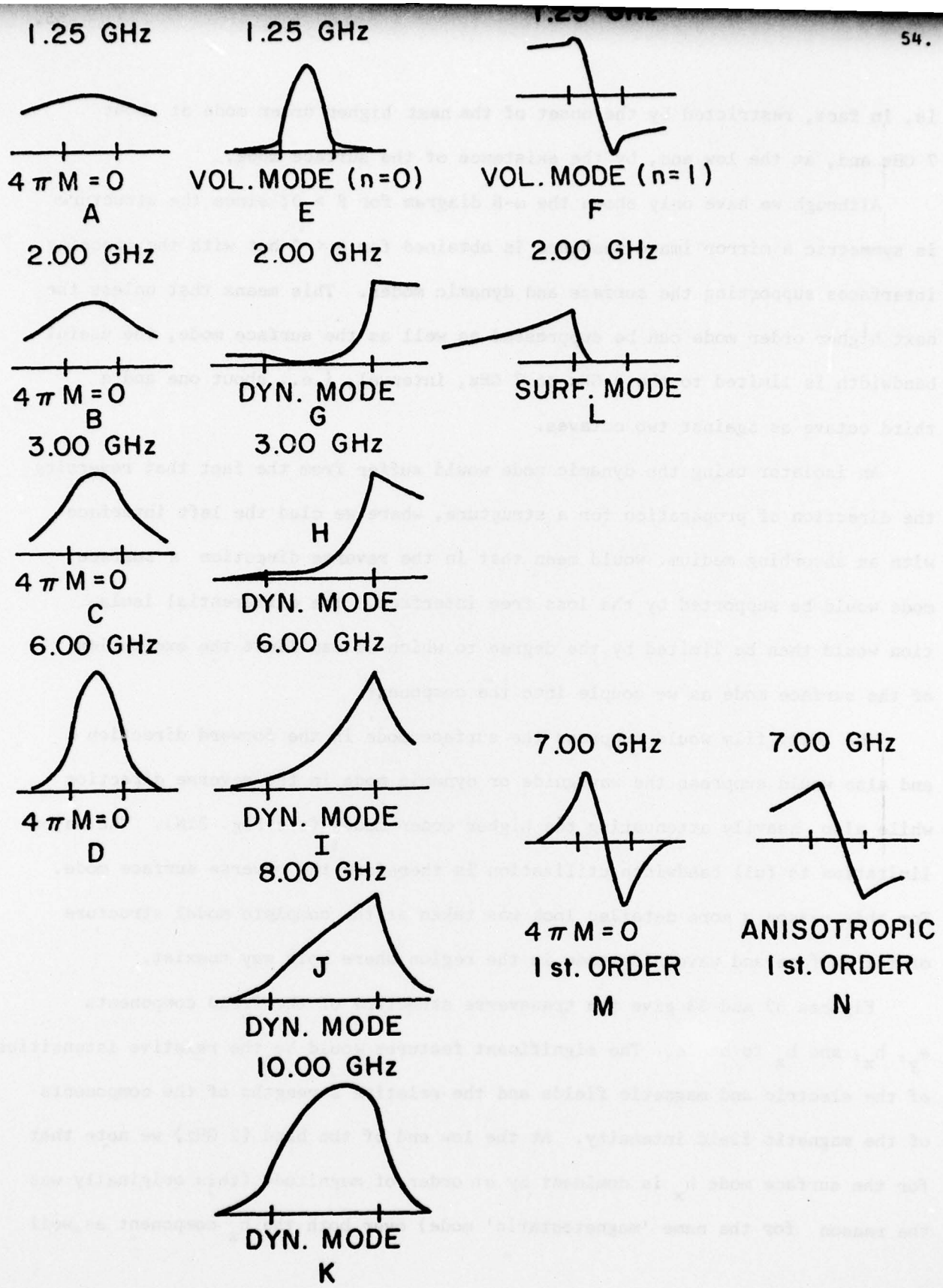

Figure 31 - Transverse electric field distributions pertaining to the lettered dots of Figure 30.

is, in fact, restricted by the onset of the next higher order mode at about 7 GHz and, at the low end, by the existence of the surface mode.

Although we have only shown the ω-β diagram for $\beta > 0$, since the structure is symmetric a mirror image response is obtained for $\beta < 0$ but with the opposing interfaces supporting the surface and dynamic modes. This means that unless the next higher order mode can be suppressed as well as the surface mode, the useful bandwidth is limited to the 3 GHz to 7 GHz, interval, i.e., about one and a third octave as against two octaves.

An isolator using the dynamic mode would suffer from the fact that reversing the direction of propagation for a structure, where we clad the left interface with an absorbing medium, would mean that in the reverse direction a surface mode would be supported by the loss free interface. The differential isolation would then be limited by the degree to which we can limit the excitation of the surface mode as we couple into the component.

The lossy film would suppress the surface mode in the forward direction and also would suppress the waveguide or dynamic mode in the reverse direction while also heavily attenuating the higher order modes (see Fig. 31N). The major limitation to full bandwidth utilization is therefore the reverse surface mode. For this reason a more detailed look was taken at the complete modal structure of the surface and waveguide mode in the region where both may coexist.

Figures 32 and 33 give the transverse structure of the field components e_y, h_x, and h_z to scale. The significant features would be the relative intensities of the electric and magnetic fields and the relative strengths of the components of the magnetic field intensity. At the low end of the band (2 GHz) we note that for the surface mode h_x is dominant by an order of magnitude (this originally was the reason for the name 'magnetostatic' mode) over both the h_z component as well

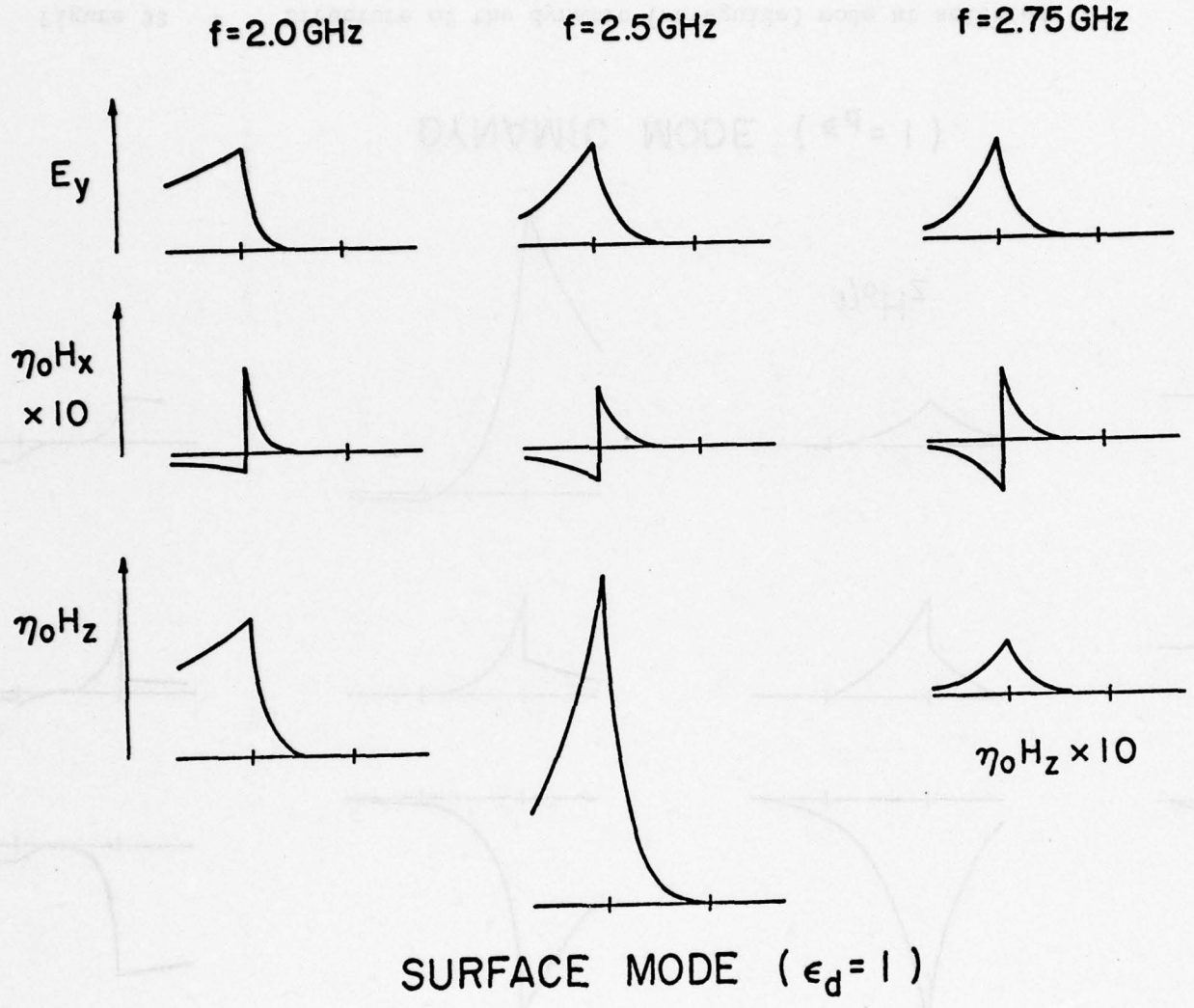

Figure 32 - Structure of the surface mode at selected frequencies. Parameters as for Figure 30.

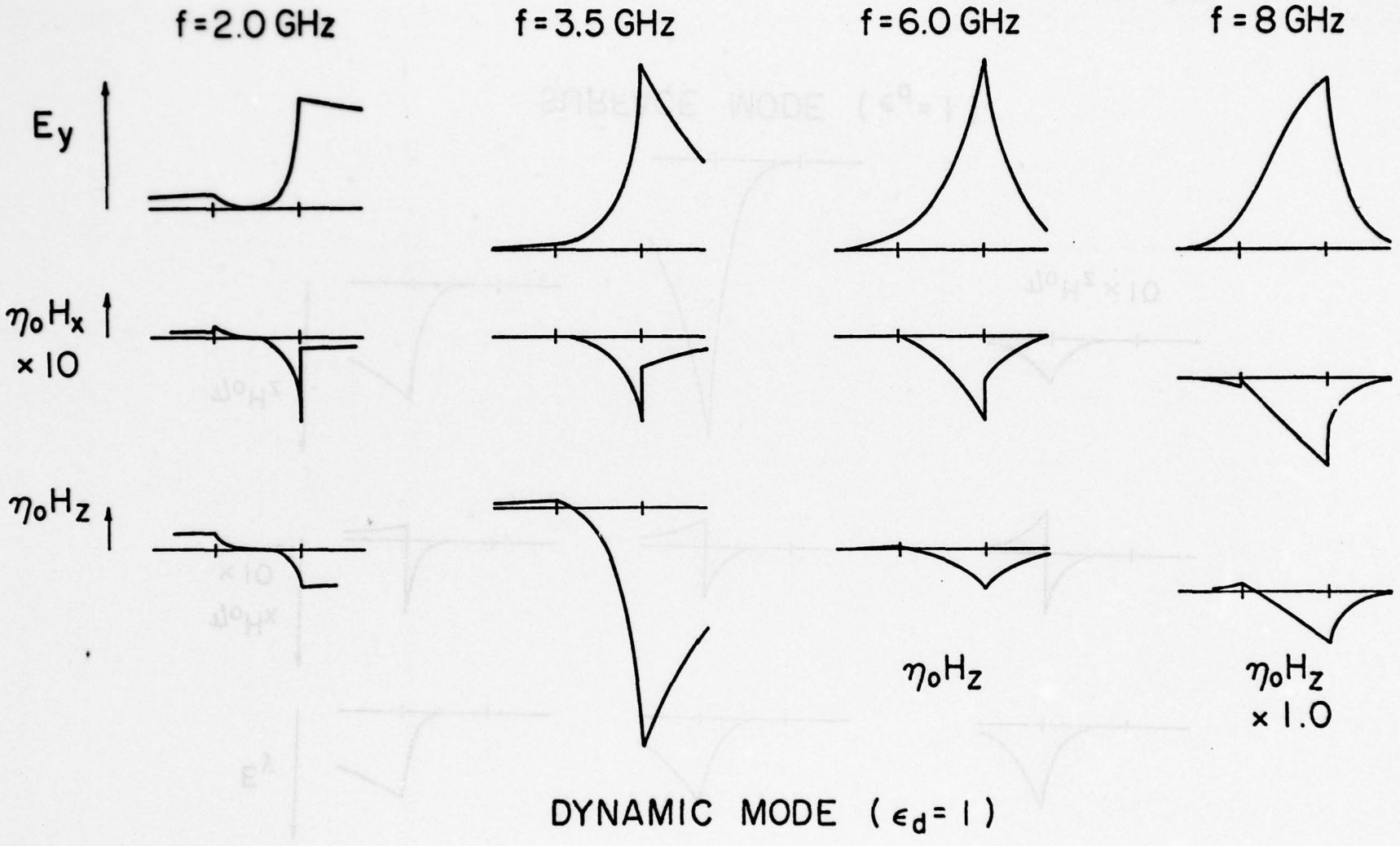

Figure 33 - Structure of the dynamic (waveguide) mode at selected frequencies for Figure 30.

as e_y noting the normalization factor η_o. The dynamic mode at this same frequency displays similar magnitude ratios and structure. Increasing the frequency to the upper end of the surface mode band does not substantially change this picture.

Data was also generated for the case where the permittivity of the dielectric regions which bound the ferrite region was increased to 4. The pertinent dispersion curves are shown in Fig. 34. Although small differences in the field structure resulted as shown in Figs. 35 and 36, these differences, if any, are not encouraging that we can effectively discriminate against the surface mode. However, since the model is rather simple, a definite conclusion must await the analysis and results of a better model such as the one shown in Fig. 28(b).

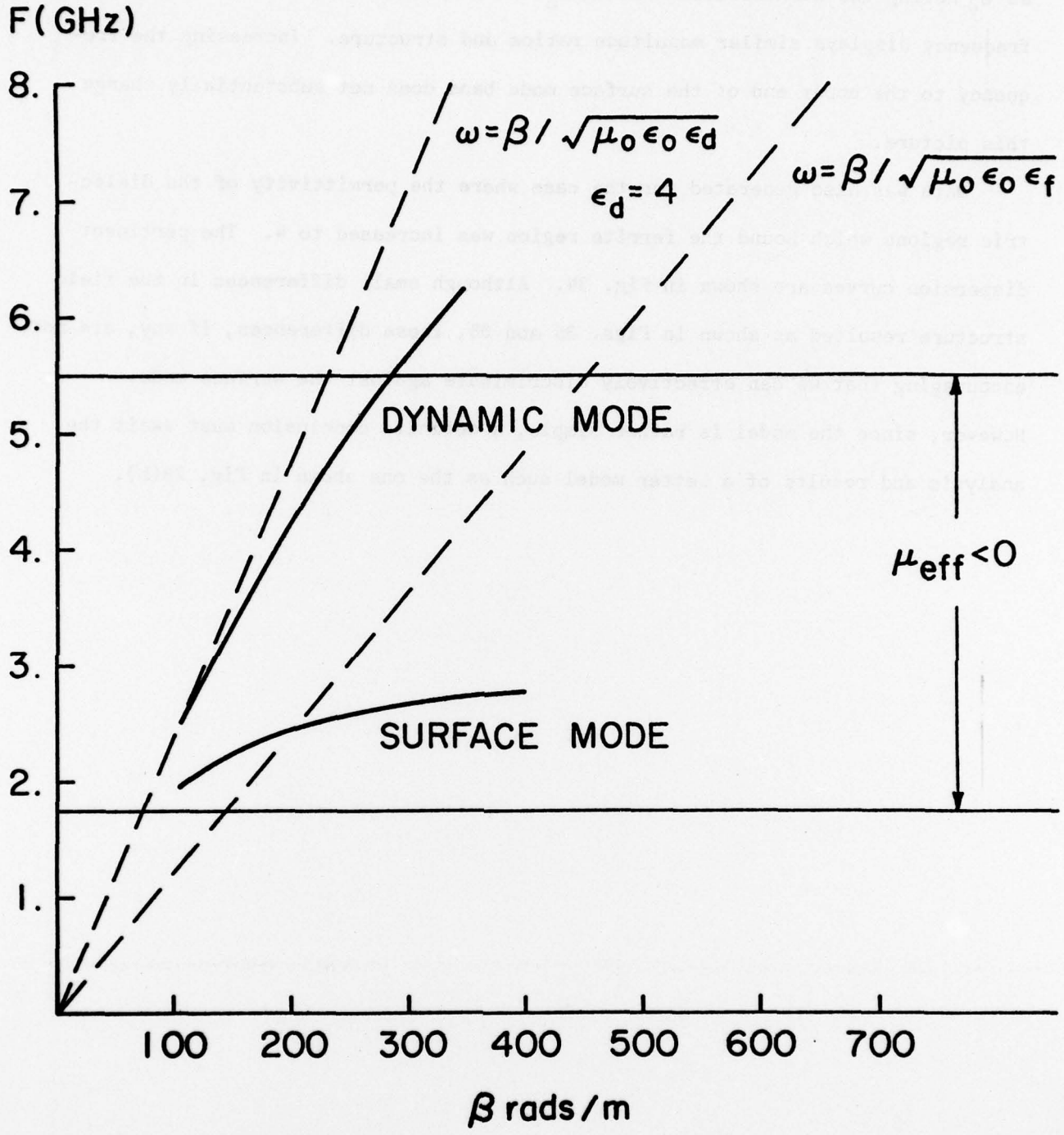

Figure 34 - Partial dispersion characteristics for the same parameters as Figure 30 but with the permittivity of the dielectric region increased to 4.

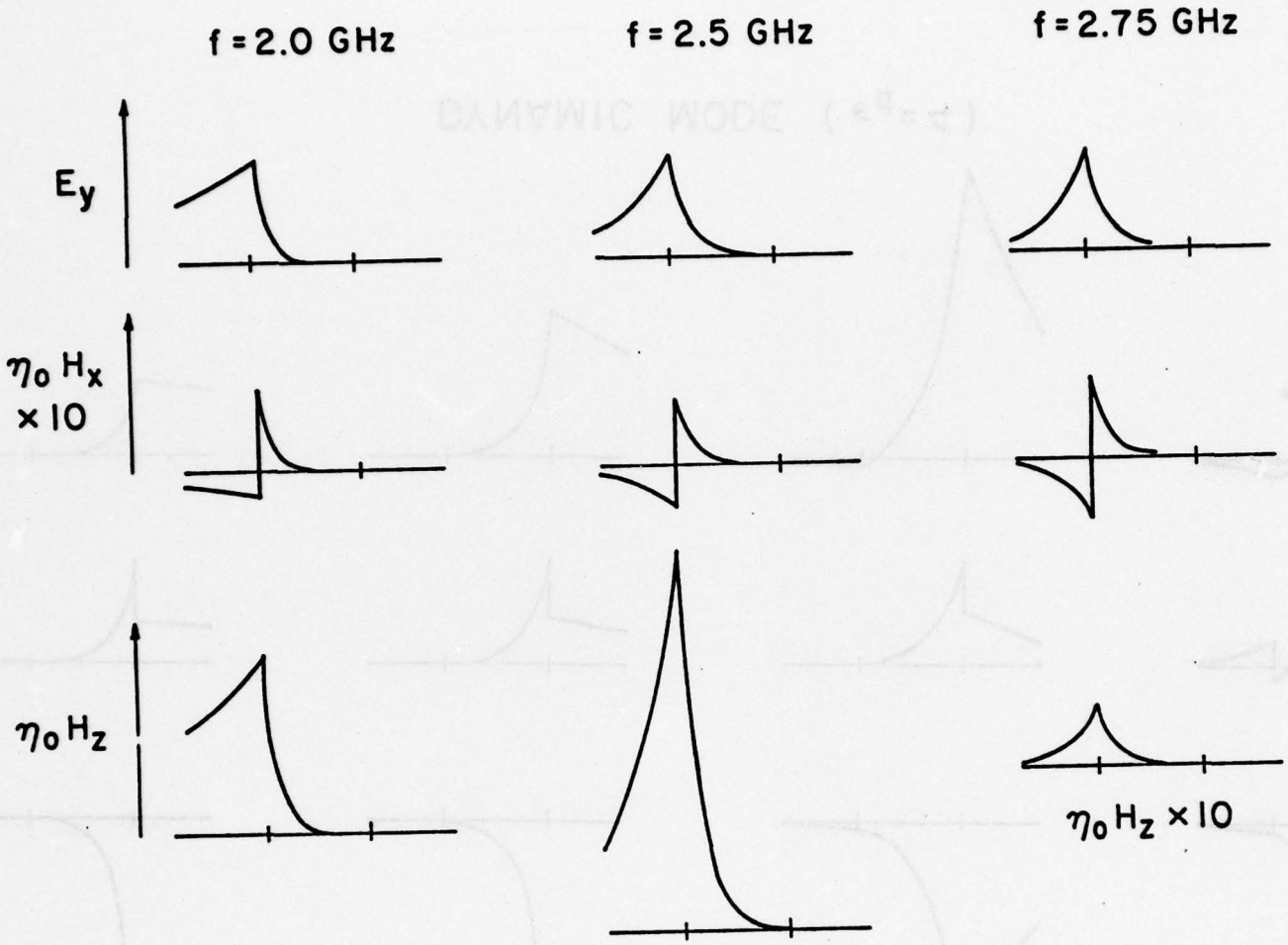

Figure 35 - Field structure of the surface mode at selected frequencies pertaining to Figure 34.

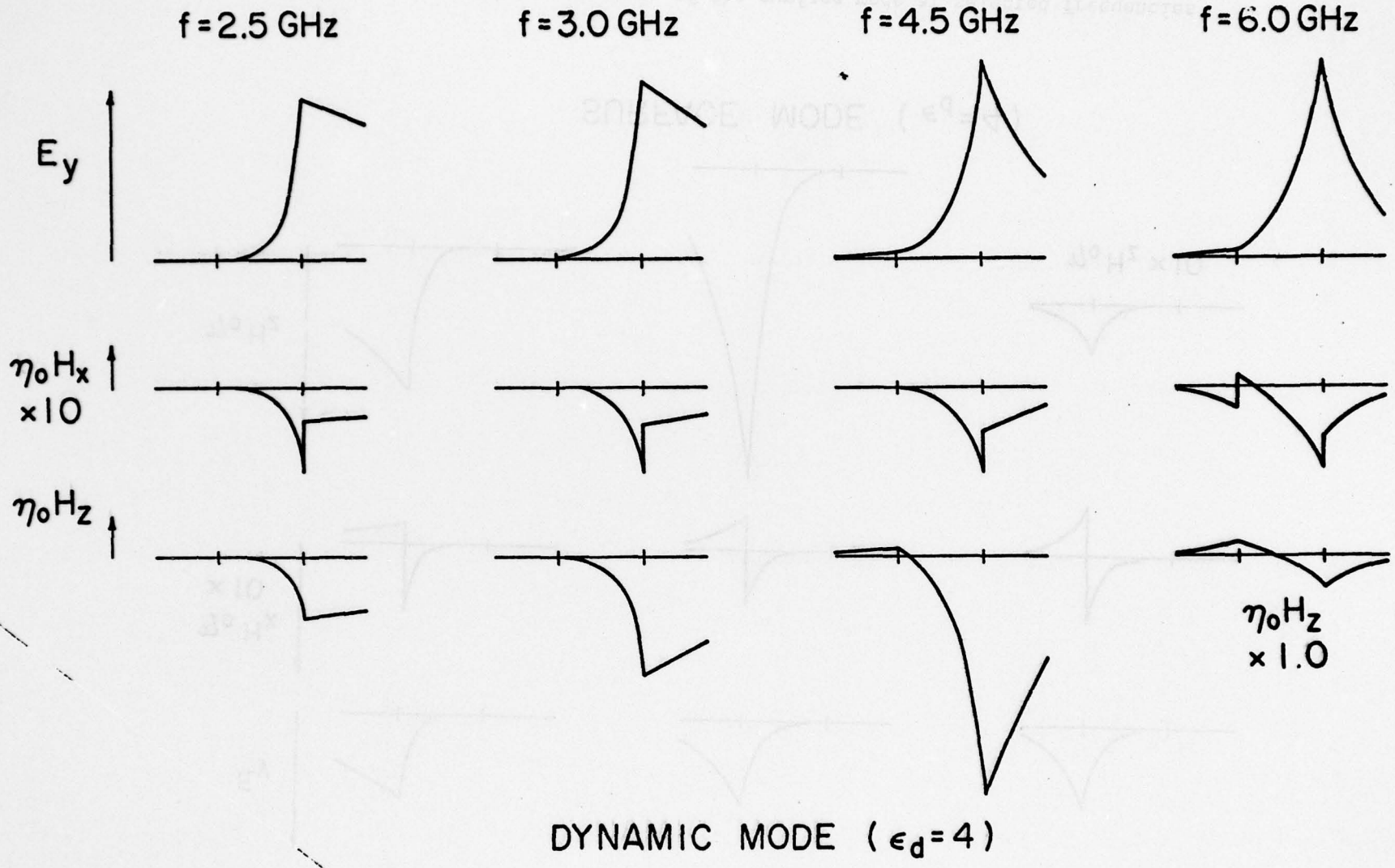

Figure 36 - Field structure of the dynamic (waveguide) mode at selected frequencies pertaining to Figure 34.

III (d) Conclusions

We have obtained the full modal spectrum of the lowest order modes (TE,n=0) for a simple model of the ferrite loaded stripline. Although quantitatively the results cannot be expected to be in good agreement with experimental results. Nevertheless, qualitatively the results should reflect accurately the behavior of such a waveguiding system.

It has become clear that components purportedly using an edge-guided (i.e., quasi-surface) mode in fact employ the field displaced quasi-TEM waveguide (or dynamic) mode. This latter mode, for even moderately wide ferrite slabs (line widths) will assume a surface mode-like structure.

Even from the limited sample calculations it appears that operation over two octaves may well become possible. However, further studies on a better model which also considers the effect of material and conductor losses must be completed before definitive conclusions can be reached.

It appears currently that the greatest difficulty will lie in suppressing unwanted surface modes while higher order modes will be quite readily suppressed using lossy films on the appropriate ferrite-dielectric interface or guide edge.

IV Bibliography

1. "Peripheral mode isolator operates from 3.5 to 11 GHz, Microwaves, Vol. 8, No. 4, pp. 64-65, April 1969.

2. M. E. Hines, "A New Microstrip Isolator and its Application to Distributed Diode Amplification", IEEE G-MTT 1970, Int. Microwave Symp., Newport Beach, CA, May 11-14, Digest of papers, pp. 304-307.

3. Gyromagnetic device having a plurality of outwardly narrowing tapering members. U.S. Patent 355,459, Inventor: R. Anderson, Jan. 12, 1971.

4. M. E. Hines, "Ferrite Phase Shifters and Multiport Circulators in Microstrip and Stripline", IEEE G-MTT 1971, Int. Microwave Symp., Washington, DC, May 16-19, Digest of papers, pp. 108-109.

5. M. E. Hines, "Reciprocal and Nonreciprocal Modes of Propagation in Ferrite Stripline and Microstrip Devices", IEEE Trans. on Microwave Theory and Tech., Vol. MTT-19, No. 5, pp. 442-451, May 1971.

6. P. deSantis, R. Roveda, "Magnetodynamic Boundary Waves," Proc. of 1971 Europ. Microwave Conf., Stockholm, Aug. 23-28, pp. C5/2:1 - C5/2:4.

7. B. Chiron, G. Forterre, C. Rannou, "Nouveaux dispositifs non reciproques à très grande largeur de bande utilisant des ones de surface electromagnétiques," L'Onde Electrique, Vol. 51, Fasc. 9, pp. 816-818, Oct. 1971.

8. L. Courtois, G. Declerq, Peurichard M., "On the Non-Reciprocal Aspect of Gyromagnetic Surface Waves", Paper presented at the Seventh Annual Conf. on Magnetism and Magnetic Materials, Chicago, IL, Nov. 16-19, 1971. Published on the Proc. of the Conf. Part. 2, pp. 1541-1545, AIP, (1972).

9. P. deSantis, F. Pucci, "Novel Type of MIC Symmetrical Three-Port Circulator, Electronics Letters, Vol. 8, pp. 12-13, Jan. 13, 1972.

10. B. Chiron, G. Forterre, "Emploi des modes de surface electromagnetiques pour la realization de dispositifs gyromagnetiques a très grande largeur de bande", Paper presented at the Premier Seminaire Int. sur les Dispositifs Hyperfrequences a Ferrite - Toulouse, France, March 27-30, 1972.

11. M. Blanc, L. Dusson, J. Guideaux, "Etude de la function isolation a trés large bande utilisant des materiaux ferrites", Paper presented at the Premier Seminaire Int. sur les Dispositifs Hyperfrequencies a Ferrite - Toulouse, France, March 27-30, 1972.

12. M. Blanc, L. Dusson, J. Guidevaux, "Etudes de dispositifs non reciproques a ferrite a tres large bande: Premieres realizations", Revue Techniques Thomson-CSF, Vol. 4, No. 1, pp. 27-48, March 1972.

Bibliography (cont'd)

13. P. deSantis, F. Pucci, "Experiments on the Optimization of a Novel MIC Symmetrical Three-Port Circulator", IEEE G-MTT 1972 Int. Microwave Symp., Chicago, IL, Digest of papers, pp. 238-240, June 1972.

14. M. E. Hines, "Ferrite Transmission Devices Using the Edge-Guided Mode of Propagation", IEEE G-MTT, 1972 Int. Microwave Symp., Chicago, IL, Digest of Papers, pp. 236-237.

15. J. Puyhaubert, "Visualisation des ondes electromagnétiques hyperfréquence à l'aide des cristaux liquides", L'Onde Electrique, Vol. 52, No. 5, May 1972, pp. 213-217.

16. G. Cortucci, P. deSantis, "Edge-Guided Waves in Lossy Ferrite Microstrips", Proc. of 1973 Europ. Microwave Conf., Brussels, Sept. 4-7, Vol. 2, p. B9-1.

17. L. Courtois, "Propagation oblique des ondes electromagnetiques dans un lame de ferrite aimanté parallélement à ses faces", Electronica y Fisica Aplicada, Vol. 16, No. 2, pp. 286-294, 1973.

18. P. deSantis, "Dispersion Characteristics for a Ferrimagnetic Plate", Applied Physics, Vol. 2, pp. 197-200, Oct. 1973.

19. L. Courtois, B. Chiron, G. Forterre, "Propagation dans une lame de ferrite aimantée: Application a de noveaux dispositifs non reciproques a large bande", Cables et telecommuncations, No. 4, pp. 417-435, Oct. 1973.

20. L. Courtois, N. Bernard, B. Chiron, G. Forterre, "A New Edge Mode Isolator in the u.h.f. Range", Paper presented at the 1974 IEEE S-MTT Int. Microwave Symp., Atlanta, GA, June 12-14.

21. P. deSantis, "Edge Guided Modes in Ferrite Microstrip With Curved Edges," Applied Physics, Vol. 4, No. 2, pp. 167-174, Aug. 1974.

22. K. Araki, R. Koyama and Y. Naito, "A New Type Isolator Using the Edge-Guided Mode," IEEE Trans., MTT-23, pp. 321, March, 1975.

23. Y. S. Wu and F. J. Rosenbaum, "Wide Band Operation of Microstrip Circulators", IEEE SMTT Trans. MTT-22, No. 10, pp. 849-856, Oct. 1974.

24. L. K. Brundle, "Experimental Study of Magnetodynamic Edge-Guided Waves on a Microwave Ferrite Substrate", Presented at the INTERMAG 1975 Conf., London, England, April 1975.

25. P. deSantis and F. Pucci, "Symmetrical Four-Part Edge-Guided Wave Circulators", IEEE Trans. MTT-24, No. 1, pp. 10-18, Jan. 1976.

26. L. Courtois et al, "A New Edge-Mode Isolator in the Very High Frequency Range", IEEE Trans. MTT, Vol. MTT-24, No. 3, pp. 129-135, March 1976.

27. D. M. Bolle, "The Edge-Guided Mode on Ferrite Loaded Stripline", 1976 IEEE-MTT-S Int. Microwave Symp.Digest, pp. 257-259, June 1976.

Bibliography (con'td)

28. P. deSantis, "Fringing Field Effects in Edge-Guided Wave Devices", IEEE Trans. MTT-24, No. 7, pp. 409-415, July 1976.

29. K. Araki, T. Koyama and Y. Naito, "Reflection Problems in Ferrite Striplines", IEEE Trans. MTT-24, No. 8, pp. 491-498, Aug. 1976.

30. D. M. Bolle, "The Peripheral or Edge-Guided Modes on the Inhomogeneously and Homogeneously Ferrite Loaded Stripline", Sixth Europ. Microwave Conf. Digest, pp. 560-564, Rome Italy, Sept. 1976.

31. M. Dydyk, "Edge-guide: one path to wideband circulator design", Parts I-II, Microwaves, pp. 55-58, Jan. 1977, pp. 50-56, Feb. 1977.

32. T. Noguchi, "New Edge-guided Mode Isolator Using Ferromagnetic Resonance Absorption", IEEE Trans. MTT-25, No. 2, pp. 100-106, Feb. 1977.

33. P. deSantis, "High Azimuthal-Index Resonances in Ferrite MIC Disk Resonators", IEEE Trans. MTT-25, No. 5, pp. 360-367, May 1977.

34. D. M. Bolle, "The Modal Spectrum of Ferrite-Loaded Striplines", 1977 IEEE MTT-S Int. Microwave Symp. Digest, pp. 519-522, June 1977.

35. D. M. Bolle, "The Modal Spectrum of Ferrite-Loaded Striplines, II", Seventh Europ. Microwave Conf. Digest, Copenhagen, Denmark, Sept. 1977.